Atypical developmental remodeling of dopamine neurons involves AKT-GSK3β signaling and glia-mediated axon degeneration

Authors:

Xiaofan Zhang[1], Wei Chen[1], Yayu Wang[1], Xun Tu[2], Xiangyu Zhang[1], Ronald L. Davis[3], Lily Yeh Jan[1], and Yuh Nung Jan[1,4,*]

Affiliations:

[1]Department of Physiology and Howard Hughes Medical Institute, University of California at San Francisco; San Francisco, CA 94158, USA.

[2]Division of Neurobiology, Department of Molecular and Cell Biology, Helen Wills Neuroscience Institute, Howard Hughes Medical Institute, University of California, Berkeley, CA 94720, USA

[3]Department of Neuroscience, UF Scripps Institute for Biomedical Research, Jupiter, FL 33458, USA

[4]Lead contact

*Correspondence: yuhnung.jan@ucsf.edu

Summary

Neuronal remodeling is essential for sculpting neural circuits, and its disruption has been implicated in neurodevelopmental and neuropsychiatric disorders. Yet the molecular and cellular diversity of remodeling across neuron types remains incompletely understood. Here, we uncover a distinct remodeling mode in a subtype of *Drosophila* dopamine neurons (DANs) critical for learning, memory, sleep, and locomotion. Unlike the stereotypical pruning-then-regrowth paradigm, these DANs undergo a transient axon overgrowth followed by selective pruning during metamorphosis. Remarkably, DAN axon pruning proceeds independently of canonical ecdysone signaling and instead involves neuron-intrinsic AKT-GSK3β signaling and extrinsic glial activity. Disruption of AKT-GSK3β signaling alters microtubule stability and impairs glial recruitment and clearance of axonal debris. Notably, the role of AKT-GSK3β is cell-type specific, underscoring

mechanistic diversity in remodeling programs. These findings reveal an unexpected overgrowth-then-pruning developmental trajectory, establishing DANs as a powerful model to uncover the mechanisms underlying neuronal remodeling, circuit maturation, and neurodegeneration.

Introduction

Neuronal remodeling is a fundamental process that shapes the architecture and function of the nervous system during development and in response to experience[1–4]. Disruption of this process may contribute to a range of neurodevelopmental and neuropsychiatric disorders, including autism spectrum disorder and schizophrenia[3–7]. Growing evidence suggests that developmental neuronal remodeling and age-related neurodegeneration may share conserved molecular mechanisms, raising the possibility that similar pathways might govern neuronal degeneration across life stages[1,8,9].

The fruit fly *Drosophila melanogaster* has long served as a powerful model for investigating the cellular and molecular basis of neuronal remodeling. A well-characterized paradigm of developmental neuronal remodeling involves the pruning of larval-stage neurites followed by regrowth to establish adult-specific circuits during *Drosophila* metamorphosis. This stereotyped pruning-then-regrowth remodeling paradigm is exemplified in many neuron types across the central nervous system (CNS) and peripheral nervous system (PNS), including cholinergic Mushroom Body (MB) neurons, GABAergic anterior paired lateral (APL) neurons, and olfactory projection neurons (PNs) in the CNS, and dendritic arborization (da) neurons in the PNS[10–14]. Whether dopamine neurons (DANs) undergo a similar remodeling trajectory was unknown.

Neuronal remodeling is driven by a combination of intrinsic and extrinsic mechanisms. The steroid hormone ecdysone functions as an essential regulator of this process across diverse neuron types that undergo pruning-then-regrowth remodeling[10–15]. Ecdysone exerts its effects through cell-autonomously expressed ecdysone receptors and downstream pathways involving caspase signaling and the ubiquitin-proteasome system (UPS)[10,13–22]. However, whether ecdysone signaling universally governs neuronal remodeling across neuron types remains largely unknown.

Pruning of neurites during neuronal remodeling typically occurs through local degeneration, followed by debris clearance mediated by extrinsic non-neuronal cells. In the CNS, glial cells engulf and eliminate degenerating neurites from MB neurons and PNs[13,23,24]. In the PNS, epidermal cells function as primary phagocytes that remove dendritic debris from da neurons[25]. Whether DANs engage in similar remodeling dynamics or rely on comparable neuron–glia interactions during development remains an open question.

Here, we identify a previously unrecognized mode of neuronal remodeling in *Drosophila* DANs. In contrast to the stereotypical pruning-then-regrowth remodeling paradigm, DANs exhibit an atypical overgrowth-then-pruning remodeling trajectory, characterized by the transient overextension of a new axon branch from an established circuit during a narrow developmental window, which is subsequently selectively pruned to establish adult-stage circuitry. Remarkably, this pruning process occurs independently of canonical ecdysone signaling, caspase activity, and the ubiquitin-proteasome system. Instead, we identify the AKT-GSK3β signaling pathway as a critical cell-intrinsic regulator of this process. We further show that DAN axon pruning proceeds through a local degeneration mechanism that involves an interplay between AKT-GSK3β signaling, microtubule cytoskeleton, and glial activities. Given the essential roles of AKT-GSK3β signaling and glial activity in DAN degeneration in Parkinson's disease (PD), our findings raise the possibility that shared principles may link DAN pruning with disease-associated neurodegenerative processes[1,8,9,26–29].

Results:

Atypical developmental remodeling of dopamine neurons in *Drosophila*

To investigate whether dopamine neurons (DANs) undergo developmental remodeling, we focused on the PPL1 (protocerebral posterior lateral 1) cluster of DANs in the central brain of *Drosophila melanogaster* (fruit fly). The PPL1 cluster consists of approximately 12 DANs per hemisphere, which can be divided into five distinct subtypes with stereotyped innervation patterns across different compartments of the Mushroom Body (MB) axons[30,31] (Figure S1A and S1B). PPL1 DANs are essential for learning and memory, forgetting, sleep, and locomotion, thus sharing several functional and mechanistic

88 similarities with DANs in the substantia nigra pars compacta (SNc) of mammals[32–35].
89 Moreover, PPL1 DANs represent the only DAN subset that consistently undergoes
90 neurodegeneration across multiple *Drosophila* Parkinson's disease (PD) models[36–38],
91 making them an excellent system for investigating the mechanisms underlying DAN
92 development in both health and disease.

93 We used the TH-D'-Gal4 driver to label PPL1 DANs[32] and trace their development across
94 various stages. While TH-D'-Gal4 labels approximately 12 DANs that project to the
95 vertical lobe, junction, and heel regions of the MB in adult flies, we found that at the third
96 instar larval stage, it labels only 3 DAN cell bodies, whose axons predominantly innervate
97 the heel region (corresponding to the MP1 or PPL1γ1pedc region, hereafter referred to
98 as MP1) (Figure S1B). This observation aligns with previous reports indicating that TH-
99 D'-Gal4 primarily labels MP1 DANs at the third instar larval stage[39].

100 During metamorphosis, the MB lobes undergo dramatic remodeling: their larval-stage-
101 specific vertical and horizontal lobes are pruned within 18 hours after puparium formation
102 (APF), followed by regrowth of the horizontal lobe beginning around 24 hr APF to
103 establish adult-specific connectivity[12,19]. Notably, a pair of GABAergic APL neurons, which
104 innervate the MB, including the MP1 region, exhibit a comparable remodeling pattern
105 involving axon pruning and subsequent regrowth[14]. Given that both APL neurons and
106 MP1 DANs innervate the MB, and that both APL neurons and MB itself remodel within a
107 similar time frame[12,14,19], we asked whether MP1 DANs follow a comparable remodeling
108 trajectory.

109 Unexpectedly, we observed an overgrowth of DAN axons from the densely innervated
110 MP1 branch into the MB's junction region (also known as the MV1 region) between 12 hr
111 and 18 hr APF (Figure 1A and 1D-1E). However, this newly extended branch is transient
112 and is progressively pruned after 24 hr APF (Figure 1A and 1F-1H). Further analysis
113 (detailed below, Figure 2) confirmed that this structure represents an overextension of
114 axons from a single pair of MP1 DANs into the degenerating MB MV1 region (Figure 3A-
115 3B and S3A-S3B), which we designated as the MP1o branch. Notably, the MP1o branch
116 was not observed prior to 6 hr APF (Figure 1A-1C), suggesting that it emerges between
117 6 hr and 12 hr APF, and it is largely pruned by 30–36 hr APF (Figure 1A, 1G-1H).

118 Quantification of the relative area occupied by MP1/MP1o branches revealed a significant
119 increase at 12, 18, and 24 hr APF compared to 0 hr APF (Figure 1I). We further validated
120 these findings using the split-Gal4 driver MB320C, which specifically labels MP1 DANs in
121 adult flies[40], and found that it recapitulated the overgrowth phenotype at 18 hr APF (Figure
122 S1C).

123 Together, these results demonstrate that DANs undergo developmental remodeling
124 during metamorphosis. Whereas previous studies of developmental remodeling have
125 documented a stereotypical pruning-then-regrowth pattern for MB neurons, PNs, APL
126 neurons, and da neurons[10–14], DANs exhibit an atypical overgrowth-then-pruning
127 remodeling pattern characterized by an initial overgrowth phase followed by pruning
128 (Figure 1J).

129 **A single pair of DANs undergoes atypical remodeling during metamorphosis**

130 At both 0 and 18 hr APF, TH-D'-Gal4 labels approximately three cell bodies within the
131 PPL1 cluster (Figure S2A-S2B, left panels). Immunostaining with anti-tyrosine
132 hydroxylase (TH) antibodies confirmed that all three somas were TH-positive, indicating
133 they are DANs (Figure S2A-S2B, middle and right panels). We thus asked whether the
134 MP1 branch and the overextended MP1o branch originate from the same neuron or from
135 distinct neurons among the three labeled DANs.

136 To address this, we used photoactivatable GFP (C3PA-GFP)[41] to examine GFP diffusion
137 between the MP1 and MP1o branches. We reasoned that if these two branches arose
138 from the same neuron, localized photoactivation in one branch would lead to GFP
139 diffusion into the other. Consistent with this hypothesis, photoactivation of the MP1 branch
140 resulted in rapid GFP diffusion into the MP1o branch at both 18 and 24 hr APF (Figure
141 2A, 2D). In contrast, although we occasionally observed branch-like structures in the MV1
142 region resembling the MP1o branch at 0 hr APF, no GFP diffusion was detected between
143 the MP1 branch and these structures (Figure 2A), confirming that the MP1o branch is not
144 present at this earlier stage.

145 To further confirm that the MP1 and MP1o branches originate from a single DAN, we
146 tracked GFP diffusion from axons in the MP1 branch back to their somas. Time-lapse

147 imaging revealed that only one of the three DAN somas gradually accumulated GFP
148 signal at 18 hr APF (Figure 2B, 2E), indicating it is directly connected to the MP1/MP1o
149 branches. The remaining two DAN somas retained baseline levels of C3PA-GFP signal
150 (Figure 2B, 2E, soma 1 and 2).

151 Similarly, the split-Gal4 driver MB320C labeled three somas at 18 hr APF (Figure S1C),
152 consistent with TH-D'-Gal4 labeling. However, MB320C progressively lost labeling of the
153 two non-MP1 DAN somas and ultimately labeled only the single MP1 DAN in the adult
154 brain (Figure S1C, 48 hr APF and adult). The fate and function of the two non-MP1 DANs
155 remain unknown and require further investigation. Together, these findings demonstrate
156 that a single pair of MP1 DANs (one per brain hemisphere) undergoes atypical
157 developmental remodeling during *Drosophila* metamorphosis.

158 **The MP1 DAN in each hemisphere innervates both hemispheres during**
159 **development and in adulthood**

160 Surprisingly, localized photoactivation of the MP1 branch in a single hemisphere at 18 hr
161 APF led to GFP diffusion not only within the targeted hemisphere, but also into the soma
162 and axons of the MP1 DAN in the contralateral hemisphere (Figure 2B, S2C). This
163 indicates that each MP1 DAN projects its axons not only ipsilaterally within the
164 hemisphere but also contralaterally across the midline so that both hemispheres receive
165 its innervation during development.

166 To confirm this observation, we photoactivated the MP1 DAN soma in one hemisphere
167 and observed GFP diffusion into the MP1/MP1o branches in both hemispheres (Figure
168 2C, 2F), further supporting the bilateral projection pattern.

169 We next asked whether this bilateral projection pattern persists into adulthood. Using
170 MB320C-Gal4-driven C3PA-GFP expression in adult flies, photoactivation of a single
171 MP1 DAN soma again resulted in GFP diffusion into MP1 branches in both hemispheres
172 (Figure S2E-S2F), demonstrating that this bilateral connectivity is maintained beyond
173 development. Given the established roles of MP1 DANs in memory formation and
174 forgetting[40,42–45], the bilateral innervation pattern may function to coordinate dopaminergic
175 modulation across hemispheres during these cognitive processes.

176 **The MP1o branch includes axons presynaptic to the MB**

177 During developmental remodeling of MB γ neurons, the larval stage γ neuron axon lobes
178 are pruned, whereas axons in the junction (MV1) and heel/peduncle (MP1) regions are
179 left largely intact[12,19] (Figure 6E). The mechanisms that limit pruning to specific regions
180 remain unknown. Subsequently, the adult-specific γ lobe regrows from the MV1/junction
181 region[46].

182 Interestingly, we found that the MP1o branch specifically targets the MV1 region of the
183 MB, as shown by both anti-FasII and anti-nc82 (a presynaptic marker) staining at 12 and
184 18 hr APF (Figure 3A-3C and S3A-S3B). In fact, the MP1o branch appeared to be
185 attracted to the MV1 region, with its distal part confined near the MV1 boundary (Figure
186 3A, dashed line). This innervation pattern was further confirmed in single confocal
187 sections (Figure 3B). 3D reconstruction of the MP1/MP1o branch and MB axons reveals
188 that the MP1o branch broadly innervates the entire MB MV1 region (Movie 1). Thus, the
189 MP1o branch represents an overextended branch of MP1 DANs that transiently
190 innervates the degenerating but unpruned MB MV1 region during active MB remodeling.

191 To test whether the MP1o branch forms synapses with the MB, we used GFP
192 reconstitution across synaptic partners (GRASP)[47] and observed reconstituted GFP
193 signal in the MV1 region at 18 and 24 hr APF (Figure 3D, S3C). This finding suggests
194 potential synaptic contacts between the MP1o branch and MB. In addition, we detected
195 Bruchpilot:GFP (Brp-GFP), a presynaptic active zone marker[48], in the MP1o branch at 18
196 and 24 hr APF (Figure 3E, S3D), indicating that the MP1o branch possesses presynaptic
197 machinery. Together, these results suggest that the MP1o branch is likely functionally
198 integrated with the MB.

199 **Pruning of MP1 DAN axons involves glia-mediated local degeneration**

200 Axon degeneration is a hallmark of many neurodegenerative disorders. In PD, DAN axon
201 degeneration often precedes soma loss, following a “dying-back” pattern in which axons
202 degenerate progressively from distal synaptic terminals toward the cell body[49–51]. It thus
203 appears that preventing or delaying axon degeneration could be a viable strategy to slow
204 disease progression[1,52,53].

205 Axon pruning of MB γ neurons and dendrite pruning of peripheral da neurons have been
206 shown to occur via local degeneration[23–25,54,55]. To determine whether pruning of the
207 MP1o branch of MP1 DANs also involves local degeneration, we examined key hallmarks
208 of this process: axons fragmentation and phagocyte-mediated clearance of neuronal
209 debris[1,2,19,55].

210 Unlike the long axonal or dendritic tracts of MB γ neurons or class IV da (daIV)
211 neurons[19,25], the MP1o branch is short with densely intertwined axons (Figure 3A-3B),
212 making it challenging to observe stereotypical fragmentation patterns. Nevertheless, we
213 observed signs of disconnected axonal fragments at the distal end of the MP1o branch
214 at 24-36 hr APF (Figure 1F-1H), suggesting that local degeneration may take place in the
215 MP1o branch. In support of this notion, our data using *shi*^{ts}-mediated inhibition of glial
216 cells indicate that axon fragmentation occurs during pruning of the MP1o branch (Figure
217 4F, 4H).

218 Another hallmark of local degeneration is the involvement of phagocytes in engulfing and
219 clearing fragmented neuronal debris. For example, glial cells have been shown to mediate
220 MB γ neuron axon pruning by engulfing fragmented axons[23,24]. We asked whether glial
221 cells similarly participate in pruning of the MP1o branch. To address this question, we first
222 examined whether glial cells accumulate in the MP1/MP1o region during pruning, which
223 would indicate their involvement. Using an anti-Repo antibody to label glial nuclei, we
224 observed a significant increase in the number of glial cells in the MP1/MP1o branches at
225 24 and 30 hr APF compared to 18 hr APF (Figure 4A-4B).

226 Glia-mediated local degeneration also involves the active infiltration of glial processes
227 into the degenerating neuropil[23,24,56]. To investigate this possible scenario, we used
228 membrane-bound RFP driven by the glial-specific repo promoter (Red-Repo) to visualize
229 glial processes in the MP1/MP1o region. In line with the observed increase in glial cell
230 number, we detected enhanced infiltration of glial processes into the MP1/MP1o region
231 at 24 and 30 hr APF relative to 18 hr APF (Figure 4C-4D).

232 Glial processes in the MP1/MP1o region exhibited punctate morphologies (Figure 4C),
233 reminiscent of the “lumps” formed during the engulfment and degradation of degenerating
234 γ neuron axons[24,54]. This observation raised the possibility of active glial engulfment of

degenerating DAN axons, likely involving the endosomal-lysosomal pathway[23,24]. To test this possibility, we labeled endosomal-lysosomal compartments using LysoTracker and simultaneously visualized axons in the MP1/MP1o branches and glial processes. At 24 hr APF, we observed considerable number of LysoTracker-positive puncta in the MP1o region that colocalized with puncta of glial processes as well as axons in the MP1/MP1o branches (Figure 4E and S4A-S4B). Together, these findings indicate that pruning of DAN axons during metamorphosis involves glial cell-mediated local degeneration.

To further study whether glial cells are required for pruning of the MP1o branch, we blocked glial endocytic activity by targeted expression of a temperature-sensitive *shibire* (shi^{ts}) construct in glial cells (Figure 4F). *Shibire* encodes Dynamin, a GTPase essential for endocytosis, phagocytosis, and membrane trafficking[57]. Shi^{ts} functions as a dominant-negative variant at restrictive temperatures (>29°C), thereby inhibiting endocytosis and other membrane-associated processes[58]. Previous studies have shown that shi^{ts} expression in glia impairs glial process infiltration and delays MB γ lobe degeneration during developmental pruning[24].

When we shifted pupae raised at the permissive temperature (23°C) to the restrictive temperature (29°C) from ~7 hr to 24 hr APF, we observed a significant reduction in the infiltration of glial processes into the MP1/MP1o region in the shi^{ts} group compared to control (Figure 4F-4G). Additionally, we detected an increase in axon debris, appearing as punctate structures within the MP1o region in the shi^{ts} group relative to the control (Figure 4F and 4H), suggestive of impaired glia-mediated engulfment or degradation process. Together, these results demonstrate that pruning of MP1 DAN axons during metamorphosis is driven by a glia-mediated local axon degeneration pathway.

Canonical ecdysone signaling is dispensable for MP1 DAN axon pruning

We next sought to investigate the cell-autonomous mechanisms underlying pruning of the MP1o branch. Ecdysone signaling is well-established as a key regulator of developmental pruning in various neuron types[10,12–15]. To test whether ecdysone signaling could similarly mediate DAN axon pruning, we expressed a dominant-negative form of the ecdysone receptor isoform B1 (EcR-B1-DN) specifically in MP1 DANs using MB320C-Gal4 and

264 examined the fate of the MP1o branch. If ecdysone signaling were required for pruning,
265 we would expect the MP1o branch to persist into adulthood upon EcR-B1-DN expression.

266 To our surprise, expression of EcR-B1-DN did not impair MP1o pruning, as axons in the
267 MP1o branch were not detected in adult flies (Figure 5A). As a positive control validating
268 the functionality of the construct, expression of EcR-B1-DN in MB γ neurons robustly
269 blocked γ lobe pruning (Figure S5A). Moreover, expression of a DN form of the EcR-A
270 isoform (EcR-A-DN) did not disrupt MP1o pruning (Figure 5B). These findings made us
271 wonder whether MP1 DANs express significant levels of ecdysone receptors.

272 EcR-B1 or EcR-A proteins are known to be expressed in MB γ neurons, da neurons, and
273 APL neurons at the onset of metamorphosis, where they play essential roles in
274 developmental remodeling[10,12,14]. However, using antibody staining, we did not detect
275 EcR-B1 or EcR-A protein expression above background levels in MP1 DAN cell bodies
276 at 0, 18, or 24 hr APF (Figure 5C-5D). In contrast, robust EcR-B1 expression was
277 observed in other brain regions (Figure S5B), confirming the reliability of our antibody
278 staining. Although we cannot exclude low-level expression below detection thresholds,
279 the absence of detectable EcR proteins in MP1 DANs is consistent with our genetic data
280 indicating that EcR signaling is not required for MP1o pruning.

281 Together, these findings indicate that canonical ecdysone signaling is dispensable for
282 pruning of the MP1o branch. While most neurons may rely on an ecdysone-dependent
283 remodeling program, MP1 DANs appear to undergo axon pruning through an ecdysone-
284 independent mechanism.

285 **Genetic screen reveals that AKT-GSK3β signaling is involved in MP1 DAN axon**
286 **pruning**

287 Although caspase activity and the UPS have been shown to be essential for
288 developmental remodeling[17–19,21], we found that MP1o pruning proceeds normally despite
289 perturbations to these pathways. Specifically, expression of a dominant-negative form of
290 the initiator caspase Dronc (Dronc-DN), as well as overexpression of the caspase
291 inhibitors p35 or DIAP1 – manipulations known to block dendrite pruning in da neurons[17]
292 – did not impair MP1o pruning (Figure S5C-S5E). Similarly, RNAi knockdown of Uba1 or

293 Cullin1 (core components of the UPS), which effectively blocks daIV dendrite pruning[21],
294 had no detectable effect on MP1o pruning (Figure S5F-S5G). Although we cannot exclude
295 the possibility that the lack of pruning phenotype may result from insufficient RNAi
296 efficiency, these findings suggest that caspase activity and UPS signaling are not
297 essential for MP1 DAN axon pruning.

298 To identify molecular pathways required for DAN axon pruning, we performed a targeted
299 genetic screen of over 200 fly lines encompassing ~60 candidate genes implicated in
300 neural development and remodeling. This screen revealed a critical role for GSK3β
301 (Shaggy, Sgg in *Drosophila*) in DAN axon pruning. Expression of a dominant-negative
302 form of GSK3β (GSK3β-DN), which mimics GSK3β inhibition, led to a pronounced
303 pruning defect, with persistent axons in the MP1o branch detectable in adult flies (Figure
304 6A-6B). Given that the GSK3β activity is negatively regulated by AKT[59–61], we asked
305 whether elevated AKT activity similarly impacts pruning. We found that expression of a
306 constitutively active form of AKT (AKT-CA) in MP1 DANs also disrupted MP1o pruning
307 (Figure 6C). In contrast, expression of constitutively active S6K1, a downstream effector
308 of mTORC1[62], did not affect pruning (Figure 6D). These findings suggest a role for AKT-
309 GSK3β signaling, but not mTORC1, in DAN axon pruning.

310 **Differential roles of AKT-GSK3β signaling in neuronal remodeling**

311 We next asked whether AKT-GSK3β signaling is similarly involved in neuronal remodeling
312 in other neuron types, such as MB γ neurons and daIV neurons. We found that expression
313 of AKT-CA or GSK3β-DN in MB γ neurons did not impair γ neuron axon pruning at 18 hr
314 APF (Figure 6E-6F), consistent with previous reports that AKT is not required for γ neuron
315 pruning[16]. Unexpectedly, AKT-CA expression appeared to enhance γ neuron axon
316 pruning, as the distal tips of unpruned γ lobes—clearly visible in controls—was barely
317 detectable in AKT-CA brains (Figure 6E-6F, arrow). Quantification of GFP-labeled pixels
318 confirmed a significant reduction in signal at the distal tip of the vertical lobes in AKT-CA
319 brains compared to wild type (Figure 6H). Additionally, we observed a significant
320 enlargement of the MB junction/MV1 region in AKT-CA flies (Figure 6F, arrowhead, and
321 6I). These phenotypes were not observed in GSK3β-DN brains (Figure 6G-6I), suggesting
322 that AKT and GSK3β may play distinct roles in γ neuron remodeling.

323 Although RNAi knockdown of AKT has been reported to rescue dendrite pruning defects
324 caused by Cullin1 knockdown in daIV neurons[63], we found that AKT-CA expression did
325 not impair daIV dendrite pruning at 18 hr APF (Figure S6A-S6B), possibly due to context
326 dependent differences in AKT activities. In contrast, expression of GSK3β-DN significantly
327 disrupted daIV dendrite pruning (Figure S6A-S6B), consistent with previous findings[64].
328 Together, these results reveal the differential roles of AKT-GSK3β signaling in the
329 developmental remodeling of distinct neuron types.

330 **Crosstalk between intrinsic AKT-GSK3β signaling and extrinsic glial activity**
331 **during MP1 DAN axon degeneration**

332 Developmental remodeling involves coordinated interactions between cell-autonomous
333 and non-cell-autonomous mechanisms. To explore potential crosstalk between intrinsic
334 AKT-GSK3β signaling and extrinsic glial responses during MP1o pruning, we analyzed
335 glial dynamics across pruning stages in AKT-CA and GSK3β-DN backgrounds. At 18 hr
336 APF, both AKT-CA and GSK3β-DN brains exhibited a reduction in the number of glial
337 cells in the MP1/MP1o region compared to controls, while glial process infiltration
338 remained largely unchanged (Figure S7A). By 24 hr APF, however, both glial cell
339 number and process infiltration were significantly reduced in AKT-CA and GSK3β-DN
340 brains (Figure 7A-7D). These reductions persisted through 30 hr APF in the GSK3β-DN
341 group and trended toward significance in the AKT-CA group (Figure S7B). Together,
342 these findings suggest that AKT-GSK3β signaling suppresses local glial responses
343 during MP1 DAN axon degeneration, revealing a potential regulatory interaction
344 between intrinsic neuronal pathways and extrinsic glial-mediated pruning mechanisms.

345 **AKT-GSK3β signaling regulates microtubule cytoskeleton dynamics during DAN**
346 **axon degeneration**

347 To investigate how AKT-GSK3β signaling may influence DAN axon pruning, we
348 examined its role in regulating microtubule cytoskeleton integrity, which is known to be
349 disrupted prior to glial engulfment in other developmental pruning contexts: In both MB γ
350 neurons and daIV neurons, early microtubule disruption is a hallmark of neural
351 degeneration, with glial engulfment occurring only after microtubule cytoskeleton
352 breakdown[19,54,55,64].

353 Using GFP-tagged αTub84B (GFP-αTub84B) as a marker, we first assessed microtubule
354 dynamics in the MP1/MP1o branches during pruning. At 12 hr APF, GFP-αTub84B signal
355 was robustly detected in the MP1o branch, with strong expression in its distal portion
356 (using the unpruned MB junction/MV1 region as reference) (Figure 7E). However, by 18
357 and 24 hr APF, the GFP-αTub84B intensity progressively diminished in the MP1o branch
358 (Figure 7E-7F), consistent with microtubule breakdown during the early phase of axon
359 degeneration[19,54].

360 To determine whether AKT-GSK3β signaling modulates this process, we expressed AKT-
361 CA or GSK3β-DN in MP1 DANs and quantified GFP-αTub84B levels. Both manipulations
362 resulted in significantly elevated GFP-αTub84B signal in the distal MP1o region compared
363 to controls (Figure 7G-7H), suggesting that AKT-GSK3β signaling stabilizes microtubule
364 cytoskeleton during degeneration of MP1 DAN axons. Together, these findings suggest a
365 model that AKT-GSK3β signaling cell-autonomously regulates microtubule cytoskeleton
366 breakdown, thereby modulating glial engagement during DAN axon degeneration.

367 **Discussion**

368 **Atypical developmental remodeling of DANs**

369 This study identifies a previously uncharacterized mode of neuronal remodeling in
370 dopamine neurons (DANs) of *Drosophila melanogaster*. In contrast to the stereotypical
371 pruning-then-regrowth remodeling paradigm observed in most neuron types – including
372 MB neurons, APL neurons, PNs, and daIV neurons[10–14] – MP1 DANs follow an atypical
373 overgrowth-then-pruning trajectory (Figure 1 and S8). This remodeling trajectory is
374 particularly striking given that both MP1 DANs and APL neurons innervate the MB, yet
375 exhibit opposite temporal patterns of remodeling. This atypical mode of remodeling of
376 DAN axons represents a notable deviation from established paradigms and underscores
377 the heterogeneity and complexity of neuronal remodeling programs in the developing
378 brain.

379 The MP1o branch emerges within a narrow developmental window and targets the MB
380 MV1, a region known to be spared during MB γ neuron pruning[12,19]. The MP1o branch
381 exhibits presynaptic markers and potential synaptic contacts with MB, suggesting that it

may be functionally integrated, albeit transiently. These observations raise intriguing possibilities: MP1 DAN axons in the MP1o branch may transiently modulate MB circuit activity, provide scaffolding for subsequent MB connectivity, or serve as a checkpoint to ensure MB pruning or regrowth fidelity.

Pruning independent of canonical ecdysone signaling

Our results indicate that MP1 DANs prune independently of the canonical ecdysone–EcR signaling pathway (Figure 5). This is in stark contrast to most remodeling neurons in *Drosophila*, including MB neurons, PNs, APL neurons, da neurons, and thoracic ventral (Tv) neurons, which show EcR expression and rely on ecdysone signaling to initiate remodeling[10,12–15]. A recent study reports that pruning of Beat-Va_M neurons in the ventral nerve cord (VNC) of *Drosophila* is also ecdysone-independent, although EcR expression is detected in these neurons[65]. In contrast, our data indicate that neither EcR-B1 nor EcR-A is detectable in MP1 DANs. While we cannot fully exclude the possibility that MP1 DANs may respond to ecdysone at levels below our detection threshold or with distinct sensitivity compared to other neuron types, our results nonetheless argue that pruning of MP1 DANs proceeds through mechanisms distinct from the canonical ecdysone-EcR pathway. Together, these findings point to neuron-type–specific pruning triggers and underscore the diversity of remodeling logic across the nervous system[1,2,8,16].

Role of AKT-GSK3β signaling in DAN axon pruning

Our genetic screen revealed a critical role for AKT-GSK3β signaling in DAN remodeling (Figure 6). Inhibition of GSK3β or constitutive activation of AKT impairs pruning of the MP1o branch, supporting a model in which the proper regulation of AKT and GSK3β activity is essential for timely DAN axon elimination.

Mechanistically, we find that AKT-GSK3β signaling modulates microtubule cytoskeleton dynamics during pruning. Pruning of the MP1o branch is accompanied by progressive microtubule disassembly, a hallmark of early axonal degeneration. Expression of AKT-CA or GSK3β-DN preserves microtubule integrity and inhibits pruning, indicating that cytoskeletal destabilization is a prerequisite for MP1 DAN axon degeneration. Our findings support a model in which AKT-GSK3β regulates the pruning process by

411 modulating microtubule destabilization—a known prerequisite for local axon
412 degeneration[2,19,54].

413 **Context-dependent roles of AKT-GSK3β in neuronal remodeling**

414 The role of AKT-GSK3β signaling in neuronal remodeling appears to be neuron type-
415 specific. This pathway is involved in MP1 DAN axon pruning but is dispensable in MB γ
416 neurons and only partially required in da neuron remodeling (Figure 6). These findings
417 highlight the context-dependent deployment of shared signaling pathways across distinct
418 neuronal populations. AKT-GSK3β signaling may thus serve specialized functions
419 depending on the developmental timing, neurite architecture, and extrinsic cellular
420 environment of the remodeling neurons[2,8,16,20,55,66].

421 **Glia-mediated pruning of DAN axons**

422 In parallel to cell-intrinsic mechanisms, we demonstrate that pruning of MP1 DAN axons
423 involves glia-mediated local degeneration and clearance (Figure 4). Glial cells
424 accumulate in the MP1/MP1o region during the pruning window and extend processes
425 into the region with degenerating axons. Lysosomal markers are enriched within glial
426 processes and colocalize with DAN axon fragments, suggestive of active phagocytosis of
427 degenerating neurites. Inhibition of glial endocytic function via expression of temperature-
428 sensitive *shi*^{ts} impairs pruning and leads to accumulation of axonal debris, consistent with
429 a requirement for glial engulfment in axon clearance. These observations are similar to
430 those in MB γ neuron and da neuron pruning, where glial or epidermal cells act as
431 phagocytes for debris engulfment and clearance[23–25,54].

432 **Crosstalk between intrinsic and extrinsic remodeling mechanisms**

433 We find that AKT-GSK3β signaling modulates not only axon-intrinsic cytoskeletal
434 remodeling but also glial behavior (Figure 7). Expression of AKT-CA or GSK3β-DN in MP1
435 DANs suppresses both glial cell accumulation and glial process infiltration into the MP1o
436 region. This suggests that cytoskeletal integrity within axons may act as a permissive cue
437 for glial engagement, either by modulating the presentation of phagocytic cues on the
438 axonal membrane or by influencing neuron-glia signaling dynamics. This is consistent
439 with observations in MB γ neurons and da neurons, where microtubule breakdown

440 precedes glial engulfment and may serve as a prerequisite for efficient clearance[23,54,55].
441 Future studies will be needed to dissect whether glia actively sense microtubule
442 disassembly or respond to other neuron-derived “find-me” or “eat-me” signals that are
443 modulated by AKT-GSK3β signaling[67–69].

444 **Implications for neurodegenerative disease**

445 The identification of AKT-GSK3β and glia-mediated local axon degeneration mechanism
446 in DAN remodeling has important implications for neurodegenerative diseases. In PD,
447 DAN axon degeneration often precedes soma loss, following a “dying-back” pattern[49,70–
448 72]. Activation of AKT or inhibition of GSK3β has been shown to suppress axon
449 degeneration and soma loss of DANs in mouse models of PD[26–29]. In addition, AKT
450 promotes axon regeneration through inhibition of GSK3β or by modulating microtubule
451 dynamics[73–75]. Growing evidence also underscores the critical role of glial cells in the
452 pathogenesis of neurodegenerative disorders, including Alzheimer's disease (AD), PD,
453 and Huntington's disease (HD)[76–78].

454 Together, these findings suggest that developmental pruning mechanisms may be co-
455 opted or dysregulated in pathological contexts. Although not the primary focus of this
456 study, our results reveal that DANs are capable of extending new axonal branches even
457 after circuit formation (i.e., during the MP1o overgrowth phase). Elucidating the molecular
458 and cellular mechanisms underlying this axon overgrowth may inform novel therapeutic
459 strategies aimed at promoting DAN axon regeneration in PD.

460 In conclusion, this study defines a novel mode of neuronal remodeling in *Drosophila*
461 DANs, integrating AKT-GSK3β–regulated microtubule destabilization with glia-mediated
462 engulfment to drive local DAN axon degeneration. These findings broaden the
463 mechanistic repertoire of developmental pruning and provides a framework for
464 investigating neuron-glia interactions in both healthy development and disease-related
465 neurodegeneration.

466

467

Acknowledgments

We thank Y.C Chang, Y. Guo, K. Li, N. C. Noyes, C.F. Teo, A. Yong, X. Ming, M. Zubia, C. Chen, P. Jin, J. Ko, and F. Xie for critical discussion; members of the Jan lab for support and feedback throughout this study; We thank S. Younger, X. Zhai, T. Cheng, and M. Y. L. Fontaine for assistance with fly work and reagents; We also thank C. Han, Janelia Research Campus, and the Bloomington *Drosophila* Stock Center for providing fly lines. This work was supported by NIH grants to Y.N.J. (R35NS097227 and R35NS137312), L.Y.J. (R35NS122110), and R.L.D. (5R35NS097224). Y.N.J. and L.Y.J. are Howard Hughes Medical Institute investigators.

Author contributions

Y.N.J. and L.Y.J. supervised the project. X.Z. conceived and initiated the project while in the laboratory of R.L.D., and continued designed and performed experiments in the laboratories of Y.N.J. and L.Y.J. X.Z. performed immunostainings, the genetic screen, photoactivation experiments, and data analysis. W.C. assisted with experiments in da neurons. Y.W. contributed to sample preparation. X.Y.Z. assisted with the genetic screen. X.T. contributed to data analysis. X.Z. wrote the manuscript with input from all authors.

Declaration of interests

The authors declare no competing interests.

References

1. Luo, L., and O'Leary, D.D.M. (2005). Axon retraction and degeneration in development and disease. Annu. Rev. Neurosci. *28*, 127–156. https://doi.org/10.1146/annurev.neuro.28.061604.135632.

2. Riccomagno, M.M., and Kolodkin, A.L. (2015). Sculpting Neural Circuits by Axon and Dendrite Pruning. Annu. Rev. Cell Dev. Biol. *31*, 779–805. https://doi.org/10.1146/annurev-cellbio-100913-013038.

3. Jan, Y.N., and Jan, L.Y. (2010). Branching out: mechanisms of dendritic arborization. Nat Rev Neurosci *11*, 316–328.

4. Faust, T.E., Gunner, G., and Schafer, D.P. (2021). Mechanisms governing activity-dependent synaptic pruning in the developing mammalian CNS. Nat. Rev. Neurosci. *22*, 657–673. https://doi.org/10.1038/s41583-021-00507-y.

5. Cocchi, E., Drago, A., and Serretti, A. (2016). Hippocampal Pruning as a New Theory of Schizophrenia Etiopathogenesis. Mol. Neurobiol. *53*, 2065–2081. https://doi.org/10.1007/s12035-015-9174-6.

6. Thomas, M.S.C., Davis, R., Karmiloff-Smith, A., Knowland, V.C.P., and Charman, T. (2016). The over-pruning hypothesis of autism. Dev. Sci. *19*, 284–305. https://doi.org/10.1111/desc.12303.

7. Ramocki, M.B., and Zoghbi, H.Y. (2008). Failure of neuronal homeostasis results in common neuropsychiatric phenotypes. Nature *455*, 912–918. https://doi.org/10.1038/nature07457.

8. Yaron, A., and Schuldiner, O. (2016). Common and Divergent Mechanisms in Developmental Neuronal Remodeling and Dying Back Neurodegeneration. Curr. Biol. *26*, R628–R639. https://doi.org/10.1016/j.cub.2016.05.025.

9. Hong, S., Beja-Glasser, V.F., Nfonoyim, B.M., Frouin, A., Li, S., Ramakrishnan, S., Merry, K.M., Shi, Q., Rosenthal, A., Barres, B.A., et al. (2016). Complement and microglia mediate early synapse loss in Alzheimer mouse models. Science *352*, 712–716. https://doi.org/10.1126/science.aad8373.

10. Kuo, C.T., Jan, L.Y., and Jan, Y.N. (2005). Dendrite-specific remodeling of Drosophila sensory neurons requires matrix metalloproteases, ubiquitin-proteasome, and ecdysone signaling. Proc. Natl. Acad. Sci. *102*, 15230–15235. https://doi.org/10.1073/pnas.0507393102.

11. Williams, D.W., and Truman, J.W. (2005). Cellular mechanisms of dendrite pruning in Drosophila: insights from in vivo time-lapse of remodeling dendritic arborizing sensory neurons. Development *132*, 3631–3642. https://doi.org/10.1242/dev.01928.

12. Lee, T., Marticke, S., Sung, C., Robinow, S., and Luo, L. (2000). Cell-Autonomous Requirement of the USP/EcR-B Ecdysone Receptor for Mushroom Body Neuronal Remodeling in *Drosophila*. Neuron *28*, 807–818. https://doi.org/10.1016/S0896-6273(00)00155-0.

13. Marin, E.C., Watts, R.J., Tanaka, N.K., Ito, K., and Luo, L. (2005). Developmentally programmed remodeling of the Drosophilaolfactory circuit. Development *132*, 725–737. https://doi.org/10.1242/dev.01614.

14. Mayseless, O., Berns, D.S., Yu, X.M., Riemensperger, T., Fiala, A., and Schuldiner, O. (2018). Developmental Coordination during Olfactory Circuit Remodeling in *Drosophila*. Neuron *99*, 1204-1215.e5. https://doi.org/10.1016/j.neuron.2018.07.050.

15. Schubiger, M., Wade, A.A., Carney, G.E., Truman, J.W., and Bender, M. (1998). Drosophila EcR-B ecdysone receptor isoforms are required for larval molting and for neuron remodeling during metamorphosis. Development *125*, 2053–2062. https://doi.org/10.1242/dev.125.11.2053.

16. Yu, F., and Schuldiner, O. (2014). Axon and dendrite pruning in *Drosophila*. Curr. Opin. Neurobiol. *27*, 192–198. https://doi.org/10.1016/j.conb.2014.04.005.

17. Williams, D.W., Kondo, S., Krzyzanowska, A., Hiromi, Y., and Truman, J.W. (2006). Local caspase activity directs engulfment of dendrites during pruning. Nat. Neurosci. *9*, 1234–1236. https://doi.org/10.1038/nn1774.

18. Kuo, C.T., Zhu, S., Younger, S., Jan, L.Y., and Jan, Y.N. (2006). Identification of E2/E3 Ubiquitinating Enzymes and Caspase Activity Regulating Drosophila Sensory Neuron Dendrite Pruning. Neuron *51*, 283–290. https://doi.org/10.1016/j.neuron.2006.07.014.

19. Watts, R.J., Hoopfer, E.D., and Luo, L. (2003). Axon pruning during Drosophila metamorphosis: evidence for local degeneration and requirement of the ubiquitin-proteasome system. Neuron *38*, 871–885.

20. Awasaki, T., Huang, Y., O'Connor, M.B., and Lee, T. (2011). Glia instruct developmental neuronal remodeling through TGF-Î 2 signaling. Nat. Neurosci. *14*, 821–823. https://doi.org/10.1038/nn.2833.

21. Furusawa, K., Ishii, K., Tsuji, M., Tokumitsu, N., Hasegawa, E., and Emoto, K. (2023). Presynaptic Ube3a E3 ligase promotes synapse elimination through down-regulation of BMP signaling. Science *381*, 1197–1205. https://doi.org/10.1126/science.ade8978.

22. Zheng, X., Wang, J., Haerry, T.E., Wu, A.Y.H., Martin, J., O'Connor, M.B., Lee, C.H.J., and Lee, T. (2003). TGF-β signaling activates steroid hormone receptor expression during neuronal remodeling in the Drosophila brain. Cell *112*, 303–315. https://doi.org/10.1016/S0092-8674(03)00072-2.

23. Watts, R.J., Schuldiner, O., Perrino, J., Larsen, C., and Luo, L. (2004). Glia engulf degenerating axons during developmental axon pruning. Curr. Biol. *14*, 678–684. https://doi.org/10.1016/j.cub.2004.03.035.

24. Awasaki, T., and Ito, K. (2004). Engulfing action of glial cells is required for programmed axon pruning during Drosophila metamorphosis. Curr. Biol. *14*, 668–677. https://doi.org/10.1016/j.cub.2004.04.001.

25. Han, C., Song, Y., Xiao, H., Wang, D., Franc, N.C., Yeh Jan, L., and Jan, Y.N. (2014). Epidermal Cells Are the Primary Phagocytes in the Fragmentation and Clearance of Degenerating Dendrites in Drosophila. Neuron *81*, 544–560. https://doi.org/10.1016/j.neuron.2013.11.021.

26. Cheng, H.-C., Kim, S.R., Oo, T.F., Kareva, T., Yarygina, O., Rzhetskaya, M., Wang, C., During, M., Talloczy, Z., Tanaka, K., et al. (2011). Akt Suppresses Retrograde Degeneration of Dopaminergic Axons by Inhibition of Macroautophagy. J. Neurosci. *31*, 2125–2135. https://doi.org/10.1523/JNEUROSCI.5519-10.2011.

27. Ries, V., Henchcliffe, C., Kareva, T., Rzhetskaya, M., Bland, R., During, M.J., Kholodilov, N., and Burke, R.E. (2006). Oncoprotein Akt/PKB induces trophic effects in murine models of Parkinson's disease. Proc. Natl. Acad. Sci. *103*, 18757–18762. https://doi.org/10.1073/pnas.0606401103.

28. Wang, W., Yang, Y., Ying, C., Li, W., Ruan, H., Zhu, X., You, Y., Han, Y., Chen, R., Wang, Y., et al. (2007). Inhibition of glycogen synthase kinase-3β protects dopaminergic neurons from MPTP toxicity. Neuropharmacology *52*, 1678–1684. https://doi.org/10.1016/j.neuropharm.2007.03.017.

29. Morales-García, J.A., Susín, C., Alonso-Gil, S., Pérez, D.I., Palomo, V., Pérez, C., Conde, S., Santos, A., Gil, C., Martínez, A., et al. (2013). Glycogen Synthase Kinase-3 Inhibitors as Potent Therapeutic Agents for the Treatment of Parkinson Disease. ACS Chem. Neurosci. *4*, 350–360. https://doi.org/10.1021/cn300182g.

30. Mao, Z., and Davis, R.L. (2009). Eight different types of dopaminergic neurons innervate the Drosophila mushroom body neuropil: anatomical and physiological heterogeneity. Front. Neural Circuits *3*.

31. Aso, Y., Hattori, D., Yu, Y., Johnston, R.M., Iyer, N.A., Ngo, T.-T., Dionne, H., Abbott, L., Axel, R., Tanimoto, H., et al. (2014). The neuronal architecture of the mushroom body provides a logic for associative learning. eLife *3*, e04577. https://doi.org/10.7554/elife.04577.

32. Liu, Q., Liu, S., Kodama, L., Driscoll, M.R., and Wu, M.N. (2012). Two dopaminergic neurons signal to the dorsal fan-shaped body to promote wakefulness in Drosophila. Curr Biol *22*, 2114–2123. https://doi.org/10.1016/j.cub.2012.09.008.

33. Marquis, M., and Wilson, R.I. (2022). Locomotor and olfactory responses in dopamine neurons of the *Drosophila* superior-lateral brain. Curr. Biol. *32*, 5406-5414.e5. https://doi.org/10.1016/j.cub.2022.11.008.

34. Claridge-Chang, A., Roorda, R.D., Vrontou, E., Sjulson, L., Li, H., Hirsh, J., and Miesenbock, G. (2009). Writing memories with light-addressable reinforcement circuitry. Cell *139*, 405–415. https://doi.org/10.1016/j.cell.2009.08.034.

35. Berry, J.A., Cervantes-Sandoval, I., Chakraborty, M., and Davis, R.L. (2015). Sleep Facilitates Memory by Blocking Dopamine Neuron-Mediated Forgetting. Cell *161*, 1656–1667. https://doi.org/10.1016/j.cell.2015.05.027.

36. Whitworth, A.J., Theodore, D.A., Greene, J.C., Beneš, H., Wes, P.D., and Pallanck, L.J. (2005). Increased glutathione S-transferase activity rescues dopaminergic neuron loss in a Drosophila model of Parkinson's disease. Proc. Natl. Acad. Sci. *102*, 8024–8029. https://doi.org/10.1073/pnas.0501078102.

37. Coulom, H., and Birman, S. (2004). Chronic Exposure to Rotenone Models Sporadic Parkinson's Disease in Drosophila melanogaster. J. Neurosci. *24*, 10993–10998. https://doi.org/10.1523/JNEUROSCI.2993-04.2004.

38. Park, J., Lee, S.B., Lee, S., Kim, Y., Song, S., Kim, S., Bae, E., Kim, J., Shong, M., Kim, J.-M., et al. (2006). Mitochondrial dysfunction in Drosophila PINK1 mutants is complemented by parkin. Nature *441*, 1157–1161. https://doi.org/10.1038/nature04788.

39. Phan, A., Thomas, C.I., Chakraborty, M., Berry, J.A., Kamasawa, N., and Davis, R.L. (2019). Stromalin Constrains Memory Acquisition by Developmentally Limiting Synaptic Vesicle Pool Size. Neuron *101*, 103-118.e5. https://doi.org/10.1016/j.neuron.2018.11.003.

40. Hige, T., Aso, Y., Modi, M.N., Rubin, G.M., and Turner, G.C. (2015). Heterosynaptic Plasticity Underlies Aversive Olfactory Learning in Drosophila. Neuron *88*, 985–998. https://doi.org/10.1016/j.neuron.2015.11.003.

41. Ruta, V., Datta, S.R., Vasconcelos, M.L., Freeland, J., Looger, L.L., and Axel, R. (2010). A dimorphic pheromone circuit in Drosophila from sensory input to descending output. Nature *468*, 686–690. https://doi.org/10.1038/nature09554.

42. Zhang, X., Sabandal, J.M., Tsaprailis, G., and Davis, R.L. (2022). Active forgetting requires Sickie function in a dedicated dopamine circuit in Drosophila. Proc. Natl. Acad. Sci. *119*, e2204229119. https://doi.org/10.1073/pnas.2204229119.

43. Aso, Y., Siwanowicz, I., Bräcker, L., Ito, K., Kitamoto, T., and Tanimoto, H. (2010). Specific dopaminergic neurons for the formation of labile aversive memory. Curr. Biol. *20*, 1445–1451.

44. Berry, J.A., Cervantes-Sandoval, I., Nicholas, E.P., and Davis, R.L. (2012). Dopamine Is Required for Learning and Forgetting in Drosophila. Neuron *74*, 530–542. https://doi.org/10.1016/j.neuron.2012.04.007.

45. Aso, Y., Herb, A., Ogueta, M., Siwanowicz, I., Templier, T., Friedrich, A.B., Ito, K., Scholz, H., and Tanimoto, H. (2012). Three Dopamine pathways induce aversive odor memories with different stability. PLoS Genet. *8*, e1002768. https://doi.org/10.1371/journal.pgen.1002768.

46. Lee, T., Lee, A., and Luo, L. (1999). Development of the Drosophila mushroom bodies: sequential generation of three distinct types of neurons from a neuroblast. Development *126*, 4065–4076.

47. Feinberg, E.H., Vanhoven, M.K., Bendesky, A., Wang, G., Fetter, R.D., Shen, K., and Bargmann, C.I. (2008). GFP Reconstitution Across Synaptic Partners (GRASP) defines cell contacts and synapses in living nervous systems. Neuron *57*, 353–363. https://doi.org/10.1016/j.neuron.2007.11.030.

48. Wagh, D.A., Rasse, T.M., Asan, E., Hofbauer, A., Schwenkert, I., Dürrbeck, H., Buchner, S., Dabauvalle, M.C., Schmidt, M., Qin, G., et al. (2006). Bruchpilot, a protein with homology to ELKS/CAST, is required for structural integrity and function

of synaptic active zones in Drosophila. Neuron *49*, 833–844. https://doi.org/10.1016/j.neuron.2006.02.008.

49. Gcwensa, N.Z., Russell, D.L., Cowell, R.M., and Volpicelli-Daley, L.A. (2021). Molecular Mechanisms Underlying Synaptic and Axon Degeneration in Parkinson's Disease. Front. Cell. Neurosci. *15*.

50. Burke, R.E., and O'Malley, K. (2013). Axon degeneration in Parkinson's disease. Exp. Neurol. *246*, 72–83. https://doi.org/10.1016/j.expneurol.2012.01.011.

51. Grosch, J., Winkler, J., and Kohl, Z. (2016). Early Degeneration of Both Dopaminergic and Serotonergic Axons – A Common Mechanism in Parkinson's Disease. Front. Cell. Neurosci. *10*.

52. Coleman, M.P., and Perry, V.H. (2002). Axon pathology in neurological disease: a neglected therapeutic target. Trends Neurosci. *25*, 532–537. https://doi.org/10.1016/S0166-2236(02)02255-5.

53. Raff, M.C., Whitmore, A.V., and Finn, J.T. (2002). Axonal Self-Destruction and Neurodegeneration. Science *296*, 868–871. https://doi.org/10.1126/science.1068613.

54. Awasaki, T., Tatsumi, R., Takahashi, K., Arai, K., Nakanishi, Y., Ueda, R., and Ito, K. (2006). Essential Role of the Apoptotic Cell Engulfment Genes draper and ced-6 in Programmed Axon Pruning during Drosophila Metamorphosis. Neuron *50*, 855–867. https://doi.org/10.1016/j.neuron.2006.04.027.

55. Lee, H.-H., Jan, L.Y., and Jan, Y.-N. (2009). Drosophila IKK-related kinase Ik2 and Katanin p60-like 1 regulate dendrite pruning of sensory neuron during metamorphosis. Proc. Natl. Acad. Sci. *106*, 6363–6368. https://doi.org/10.1073/pnas.0902051106.

56. MacDonald, J.M., Beach, M.G., Porpiglia, E., Sheehan, A.E., Watts, R.J., and Freeman, M.R. (2006). The *Drosophila* Cell Corpse Engulfment Receptor Draper Mediates Glial Clearance of Severed Axons. Neuron *50*, 869–881. https://doi.org/10.1016/j.neuron.2006.04.028.

57. Orth, J.D., and McNiven, M.A. (2003). Dynamin at the actin–membrane interface. Curr. Opin. Cell Biol. *15*, 31–39. https://doi.org/10.1016/S0955-0674(02)00010-8.

58. Kitamoto, T. (2001). Conditional modification of behavior in Drosophila by targeted expression of a temperature-sensitive shibire allele in defined neurons. J Neurobiol *47*, 81–92.

59. Manning, B.D., and Cantley, L.C. (2007). AKT/PKB Signaling: Navigating Downstream. Cell *129*, 1261–1274. https://doi.org/10.1016/j.cell.2007.06.009.

60. Cross, D.A.E., Alessi, D.R., Cohen, P., Andjelkovich, M., and Hemmings, B.A. (1995). Inhibition of glycogen synthase kinase-3 by insulin mediated by protein kinase B. Nature *378*, 785–789. https://doi.org/10.1038/378785a0.

61. Hermida, M.A., Dinesh Kumar, J., and Leslie, N.R. (2017). GSK3 and its interactions with the PI3K/AKT/mTOR signalling network. Adv. Biol. Regul. *65*, 5–15. https://doi.org/10.1016/j.jbior.2017.06.003.

62. Saxton, R.A., and Sabatini, D.M. (2017). mTOR Signaling in Growth, Metabolism, and Disease. Cell *168*, 960–976. https://doi.org/10.1016/j.cell.2017.02.004.

63. Wong, J.J.L., Li, S., Lim, E.K.H., Wang, Y., Wang, C., Zhang, H., Kirilly, D., Wu, C., Liou, Y.-C., Wang, H., et al. (2013). A Cullin1-Based SCF E3 Ubiquitin Ligase Targets the InR/PI3K/TOR Pathway to Regulate Neuronal Pruning. PLOS Biol. *11*, e1001657. https://doi.org/10.1371/journal.pbio.1001657.

64. Dzaki, N., Bu, S., Lau, S.S.Y., Yong, W.L., and Yu, F. (2022). Drosophila GSK3β promotes microtubule disassembly and dendrite pruning in sensory neurons. Development *149*, dev200844. https://doi.org/10.1242/dev.200844.

65. Lehmann, K.S., Hupp, M.T., Abalde-Atristain, L., Jefferson, A., Cheng, Y.-C., Sheehan, A.E., Kang, Y., and Freeman, M.R. (2024). Astrocyte-dependent local neurite pruning in Beat-Va neurons. J. Cell Biol. *224*, e202312043. https://doi.org/10.1083/jcb.202312043.

66. Awasaki, T., and Lee, T. (2011). Orphan nuclear receptors control neuronal remodeling during fly metamorphosis. Nat. Neurosci. *14*, 6–7. https://doi.org/10.1038/nn0111-6.

67. Segawa, K., and Nagata, S. (2015). An Apoptotic ‘Eat Me’ Signal: Phosphatidylserine Exposure. Trends Cell Biol. *25*, 639–650. https://doi.org/10.1016/j.tcb.2015.08.003.

68. Ravichandran, K.S. (2010). Find-me and eat-me signals in apoptotic cell clearance: progress and conundrums. J. Exp. Med. *207*, 1807–1817. https://doi.org/10.1084/jem.20101157.

69. Ravichandran, K.S. (2011). Beginnings of a Good Apoptotic Meal: The Find-Me and Eat-Me Signaling Pathways. Immunity *35*, 445–455. https://doi.org/10.1016/j.immuni.2011.09.004.

70. Song, P., Peng, W., Sauve, V., Fakih, R., Xie, Z., Ysselstein, D., Krainc, T., Wong, Y.C., Mencacci, N.E., Savas, J.N., et al. (2023). Parkinson’s disease-linked parkin mutation disrupts recycling of synaptic vesicles in human dopaminergic neurons. Neuron *111*, 3775-3788.e7. https://doi.org/10.1016/j.neuron.2023.08.018.

71. Tagliaferro, P., and Burke, R.E. (2016). Retrograde Axonal Degeneration in Parkinson Disease. J. Park. Dis. *6*, 1–15. https://doi.org/10.3233/JPD-150769.

719 72. Volpicelli-Daley, L.A., Luk, K.C., Patel, T.P., Tanik, S.A., Riddle, D.M., Stieber, A.,
720 Meaney, D.F., Trojanowski, J.Q., and Lee, V.M.-Y. (2011). Exogenous α-Synuclein
721 Fibrils Induce Lewy Body Pathology Leading to Synaptic Dysfunction and Neuron
722 Death. Neuron *72*, 57–71. https://doi.org/10.1016/j.neuron.2011.08.033.

723 73. Song, Y., Ori-McKenney, K.M., Zheng, Y., Han, C., Jan, L.Y., and Jan, Y.N. (2012).
724 Regeneration of Drosophila sensory neuron axons and dendrites is regulated by the
725 Akt pathway involving Pten and microRNA bantam. Genes Dev. *26*, 1612–1625.
726 https://doi.org/10.1101/gad.193243.112.

727 74. Guo, X., Snider, W.D., and Chen, B. (2016). GSK3β regulates AKT-induced central
728 nervous system axon regeneration via an eIF2Bε-dependent, mTORC1-independent
729 pathway. eLife *5*, e11903. https://doi.org/10.7554/eLife.11903.

730 75. Kim, S.R., Chen, X., Oo, T.F., Kareva, T., Yarygina, O., Wang, C., During, M.,
731 Kholodilov, N., and Burke, R.E. (2011). Dopaminergic pathway reconstruction by
732 Akt/Rheb-induced axon regeneration. Ann. Neurol. *70*, 110–120.
733 https://doi.org/10.1002/ana.22383.

734 76. Wilson, D.M., Cookson, M.R., Van Den Bosch, L., Zetterberg, H., Holtzman, D.M.,
735 and Dewachter, I. (2023). Hallmarks of neurodegenerative diseases. Cell *186*, 693–
736 714. https://doi.org/10.1016/j.cell.2022.12.032.

737 77. Hanslik, K.L., Marino, K.M., and Ulland, T.K. (2021). Modulation of Glial Function in
738 Health, Aging, and Neurodegenerative Disease. Front. Cell. Neurosci. *15*.
739 https://doi.org/10.3389/fncel.2021.718324.

740 78. Glass, C.K., Saijo, K., Winner, B., Marchetto, M.C., and Gage, F.H. (2010).
741 Mechanisms Underlying Inflammation in Neurodegeneration. Cell *140*, 918–934.
742 https://doi.org/10.1016/j.cell.2010.02.016.

743 79. Han, C., Jan, L.Y., and Jan, Y.-N. (2011). Enhancer-driven membrane markers for
744 analysis of nonautonomous mechanisms reveal neuron–glia interactions in
745 Drosophila. Proc. Natl. Acad. Sci. *108*, 9673–9678.
746 https://doi.org/10.1073/pnas.1106386108.

747 80. Lee, T., and Luo, L. (1999). Mosaic analysis with a repressible cell marker for
748 studies of gene function in neuronal morphogenesis. Neuron *22*, 451–461.

749 81. Pech, U., Pooryasin, A., Birman, S., and Fiala, A. (2013). Localization of the
750 Contacts Between Kenyon Cells and Aminergic Neurons in the Drosophila
751 melanogaster Brain Using SplitGFP Reconstitution. J. Comp. Neurol. *521*, 3992–
752 4026. https://doi.org/10.1002/CNE.23388.

753 82. Yadav, S., Younger, S.H., Zhang, L., Thompson-Peer, K.L., Li, T., Jan, L.Y., and Jan,
754 Y.N. (2019). Glial ensheathment of the somatodendritic compartment regulates
755 sensory neuron structure and activity. Proc. Natl. Acad. Sci. U. S. A. *116*, 5126–
756 5134.

757 83. Jenett, A., Rubin, G.M., Ngo, T.T.B., Shepherd, D., Murphy, C., Dionne, H., Pfeiffer,
758 B.D., Cavallaro, A., Hall, D., Jeter, J., et al. (2012). A GAL4-Driver Line Resource for
759 Drosophila Neurobiology. Cell Rep. *2*, 991–1001.
760 https://doi.org/10.1016/j.celrep.2012.09.011.

761

762

RESOURCE AVAILABILITY

Further information and requests for resources and reagents should be directed to the lead contact Yuh Nung Jan (yuhnung.jan@ucsf.edu).

Materials availability

All unique reagents generated in this study are available from the lead contact.

Data and code availability

This study does not generate datasets or code.

EXPERIMENTAL MODEL AND STUDY PARTICIPANT DETAILS

Drosophila husbandry and strains

Flies were maintained on standard *Drosophila* food at 25°C, 70% relative humidity, under a 12/12 hr light/dark cycle unless otherwise specified. Pupae were collected at 2 hr intervals and aged to defined developmental stages for subsequent experiments. The following fly strains were used: w1118, TH-D'-Gal4 driver[32], MB320C-Split-Gal4 driver[40], UAS-CD4-tdTomato[79], UAS-CD4-tdGFP[79], UAS-mCD8-GFP[80], UAS-myr-GFP (BDSC #32197), UAS-myrGFP.QUAS-mtdTomato-3xHA (BDSC #77479), UAS-C3PA-GFP[41], MB-spGFP11 construct[81], UAS-spGFP1-10 construct[47], UAS-Brp-GFP (gift from Stephan Sigrist), RedRepo[82], Repo-QF2 (BDSC #66477), QUAS-shi^{ts1} (BDSC #30013), UAS-EcR-B1^{DN} (BDSC# 6872), UAS-EcR-A^{DN} (BDSC #9452), UAS-AKT^{CA} (BDSC #80935), UAS-GSK3β^{DN} (BDSC #5360), UAS-S6K^{CA} (BDSC #6913), 201y-Gal4 (BDSC #64296), PPK-Gal4 driver[79], UAS-GFP-αTub84B (BDSC #7373), UAS-Dronc^{DN} (BDSC #58992), UAS-p35 (BDSC #5073), UAS-DIAP1 (BDSC #6657), TRiP RNAi control lines (BDSC# 36303 or 36304), UAS-Uba1-RNAi (BDSC #76066), UAS-Cullin1-RNAi (BDSC #29520). Genotypes of flies in each experiment are described in Table S1.

Immunostaining

Drosophila brains were dissected and processed as previously described[42,83]. Briefly, brains were dissected in cold S2 medium (Life Technologies, Cat# 21720-024) and fixed overnight at 4°C in 1% paraformaldehyde in S2 medium. Following fixation, brains were

790 washed with PAT3 buffer [phosphate buffered saline (PBS) with 0.5% BSA and 0.5%
791 TritonX-100], blocked in 3% normal goat serum (NGS) in PAT3, and incubated with
792 primary antibodies diluted in blocking buffer (3% NGS in PAT3) for 3 hours at 23°C,
793 followed by overnight incubation at 4°C. After washing with PAT3, brains were incubated
794 with secondary antibodies in blocking buffer for 3 hours at 23°C and then at 4°C for an
795 additional 5 days. Brains were then washed with PAT3 and subsequently with 1XPBS
796 before mounting with mounting medium (Vector Laboratories, Cat# H-1000-10). Primary
797 antibodies used were: rabbit anti-GFP (1:1000, Invitrogen, Cat# A11122), chicken anti-
798 GFP (1:1000, Abcam, Cat# ab13970), rabbit anti-Dsred (1:1000, Takara Bio, Cat#
799 632496), rabbit anti-TH (1:500, Millipore, Cat# AB152), mouse monoclonal anti-FasII
800 (1:100, DSHB, 1D4, RRID:AB_528235), mouse monoclonal anti-nc82 (1:50, DSHB,
801 RRID:AB_2314866), mouse monoclonal anti-repo (1:100, DSHB, 8D12,
802 RRID:AB_528448), mouse monoclonal anti-EcR-B1 (1:50, DSHB, AD4.4,
803 RRID:AB_2154902), mouse monoclonal anti-EcR-A (1:50, DSHB, 15G1a,
804 RRID:AB_528214). Secondary antibodies used were: Alexa 488 goat anti-rabbit (1:800,
805 Invitrogen, Cat# A11008), Alexa 488 goat anti-chicken (1:800, Invitrogen, Cat# A11039),
806 Alexa 594 donkey anti-mouse (1:500, Jackson Labs, Cat# 715-585-150), Alexa 633 goat
807 anti-rabbit (1:800, Invitrogen, Cat# A21070), Alexa 633 goat anti-mouse (1:800, Invitrogen,
808 Cat# A21052). Images were collected on a Leica SP8 confocal microscope using either
809 a 10X dry or 40X oil objective, at 1024 X 1024 or 2048 X 2048-pixel resolution, with
810 excitation lasers at 488, 594, and/or 633 nm. Image analysis was performed using
811 Fiji/ImageJ.
812

813 **LysoTracker staining**

814 Drosophila brains were dissected in S2 medium at room temperature and transferred to
815 100 nM LysoTracker Deep Red (Invitrogen, Cat# L12492) diluted in S2 medium. Samples
816 were incubated for 15 min at room temperature, then washed three times with PBS before
817 imaging.
818

819 **Photoactivation of C3PA-GFP**

820 To label MP1 or MP1o branch with C3PA-GFP, brains were dissected in 1XPBS and
821 transferred to fresh 1XPBS on a microscope slide with a donut-shaped spacer. A coverslip
822 was then applied to the spacer to minimize PBS evaporation and prevent brain movement
823 during subsequent photoactivation and imaging. Prior to photoactivation, MP1 and/or
824 MP1o branches were imaged using a 10X dry objective at 1024 X 1024-pixel resolution
825 with 488 nm (for C3PA-GFP) and/or 561 nm (for tdTomato) laser excitation (designated
826 as the "Pre" image). Photoactivation was performed on a Leica SP8 microscope using a
827 405 nm laser. TdTomato signal was used to identify the MP1 or MP1o region, and a
828 circular ROI of the same size across experiments was drawn within the boundaries of the
829 MP1 or MP1o region for photoactivation. C3PA-GFP was photoactivated by scanning the
830 ROI with 4 iterations, each lasting 1.471seconds. In experiments requiring visualization
831 of GFP diffusion from axons to soma or soma to axons, the photoactivation protocol was
832 repeated every 10 or 20 minutes to enhance GFP signal for diffusion. After photoactivation,
833 the MP1, MP1o, and/or soma were imaged at defined time points using the same imaging
834 settings as that for the "Pre" image.

835 ***Shi^{ts}* experiments**

836 To inhibit dynamin function using *shi^{ts}*, pupae cultured at 23°C were shifted to 29°C from
837 approximately 7 hr APF to 24 hr APF. Pupae were dissected at 24 hr APF immediately
838 after removal from 29°C, then fixed and stained as described above.

839 **3D rendering**

840 Three-dimensional reconstruction of the MP1/MP1o branch and MB axons (Video S1)
841 was performed using Imaris software (version 10.1, Bitplane).

842 **Quantification and statistical analysis**

843 Confocal images were analyzed using Fiji/ImageJ, and statistical analyses were
844 performed in GraphPad Prism 9. The sample size for each group, *p*-values and the
845 statistical tests employed for each experiment are indicated in the figures or figure
846 legends.

To quantify the relative area occupied by MP1/MP1o (Figure 1), Z-projections were generated from confocal image stacks, and brightness and contrast were adjusted uniformly across all developmental stages. Regions within the MP1/MP1o area with signal above a defined threshold were outlined and measured in Fiji/ImageJ. The resulting area was then normalized to brain size, estimated as the distance between the left and right MP1 branches, to calculate the relative area occupied by MP1/MP1o.

To quantify C3PA-GFP fluorescence intensity before and after photoactivation (Figure 2, S2), a circular ROI of the same size was drawn around the outer boundaries of the MP1, MP1o, or soma region for each corresponding area, and the mean intensity was used for quantification.

To quantify the number of glial cells in the MP1/MP1o region, Z-projections were generated from confocal stacks. A circular ROI of the same size across all developmental stages was drawn around the outer boundaries of the MP1 and MP1o region, and the number of glial cells within the ROI was counted using Fiji/ImageJ.

To quantify glial process intensity, a Z-projection consisting of 15 optical slices (15 μm total) spanning the anterior-posterior extent of the MP1o branch was generated from confocal stacks. A circular ROI of the same size was drawn within the MP1o boundaries, and the mean intensity within the ROI was measured using Fiji/ImageJ.

To quantify GFP puncta in the *shi*^{ts} experiments (Figure 4F and 4H), a Z-projection spanning the anterior-posterior extent of the MP1o branch was generated from confocal stacks and converted to greyscale in Fiji/ImageJ. Two duplicate images were created for each projection and subjected to Gaussian blur filter with Sigma values of 1 and 2, respectively. The image with Sigma = 2 was then subtracted from the image with Sigma = 1 using the Image Calculator tool. Thresholding was then applied using the MaxEntropy algorithm, which we found to be the most reliable for distinguishing true GFP puncta from background and false-positive signals. Only GFP puncta located in the distal region of the MP1o branch were quantified, as puncta in the proximal region were predominantly false positives.

875 To quantify the size of unpruned γ lobe vertical tips and MB peduncles (Figure 6), Z-
876 projections were generated from confocal stacks, and brightness and contrast were
877 adjusted uniformly across all groups. Regions corresponding to the γ lobe vertical tip or
878 MB peduncle with signal above a defined threshold were outlined and measured using
879 Fiji/ImageJ.

880 To quantify dendrite length (Figure S6), the Simple Neurite Tracer (SNT) plugin in
881 Fiji/ImageJ was used. The total length of all traced dendrites per brain was quantified.

882 To quantify GFP–αTub84B intensity (Figure 7), a Z-projection consisting of 15 optical
883 slices (15 μm total) spanning the anterior-posterior extent of the MP1o branch was
884 generated from confocal stacks. A rectangular ROI of the same size across all
885 experimental groups was placed around the distal part of the MP1o branch using the
886 unpruned MB peduncle as reference. The mean intensity within the ROI was measured
887 using Fiji/ImageJ after background subtraction using an identical ROI placed in a
888 background region of the image.

889

890 **Table S1**

Figure	Panel	Genotype
Figure 1	B-I	TH-D'-GAL4/+; UAS-CD4-tdTomato/+
Figure 2	A-F	TH-D’-GAL4/UAS-C3PA-GFP; UAS-CD4-tdTomato/+
Figure 3	A-C	TH-D'-GAL4/+; UAS-CD4-tdTomato/+
	D	TH-D'-GAL4/+; MB-spGFP11, UAS-spGFP1-10/+
	E	TH-D’-GAL4/+; UAS-Brp-GFP/UAS-CD4-tdTomato
Figure 4	A, B	TH-D'-GAL4/+; UAS-CD4-tdGFP/+
	C, D	UAS-mCD8-GFP/+; TH-D'-GAL4/Red-Repo
	E	TH-D'-GAL4/Red-Repo; UAS-CD4-tdGFP/+
	F-H	UAS-myr-GFP, QUAS-mtdTomato-3xHA/+; TH-D'-GAL4/+ or QUAS-shi^{ts}; Repo-QF2/+
Figure 5	A	UAS-mCD8-GFP/+; UAS-EcR-B1-DN/+; MB320C-GAL4/+
	B	UAS-mCD8-GFP/+; UAS-EcR-A-DN/+; MB320C-GAL4/+
	C, D	UAS-mCD8-GFP/+; TH-D'-GAL4/+
Figure 6	A	UAS-mCD8-GFP/+;; MB320C-GAL4/+
	B	UAS-mCD8-GFP/+;; MB320C-GAL4/UAS-AKT-CA
	C	UAS-mCD8-GFP/+;; MB320C-GAL4/UAS-GSK3β-DN
	D	UAS-mCD8-GFP/+;; MB320C-GAL4/UAS-S6K-CA
	E-I	201Y-GAL4, UAS-mCD8-GFP/+, UAS-AKT-CA, or UAS-GSK3β-DN
Figure 7	A-D	UAS-mCD8-GFP/+; TH-D'-GAL4/Red-Repo; +/+, UAS-AKT-CA, or UAS-GSK3β-DN
	E, F	TH-D'-GAL4/+; UAS-GFP-αTub84B/+
	G, H	TH-D'-GAL4/+; UAS-GFP-αTub84B/+, UAS-AKT-CA, or UAS-GSK3β-DN
Figure S1	B	TH-D'-GAL4/+; UAS-CD4-tdTomato/+
	C	MB320C-GAL4/UAS-CD4-tdTomato
Figure S2	A, B	UAS-mCD8-GFP/+; TH-D'-GAL4/+

	C, D	TH-D’-GAL4/UAS-C3PA-GFP; UAS-CD4-tdTomato/+
	E, F	UAS-C3PA-GFP/+; MB320C-GAL4/UAS-CD4-tdTomato
Figure S3	A, B	TH-D'-GAL4/+; UAS-CD4-tdTomato/+
	C	TH-D'-GAL4/+; MB-spGFP11, UAS-spGFP1-10/+
	D	TH-D’-GAL4/+; UAS-Brp-GFP/UAS-CD4-tdTomato
Figure S4	A, B	TH-D'-GAL4/Red-Repo; UAS-CD4-tdGFP/+
Figure S5	A	201Y-GAL4, UAS-mCD8-GFP/UAS-EcR-B1-DN
	B	UAS-mCD8-GFP/+; TH-D'-GAL4/+
	C	UAS-mCD8-GFP/+; UAS-Dronc-DN/+; MB320C-GAL4/+
	D	UAS-mCD8-GFP/+;; MB320C-GAL4/UAS-p35
	E	UAS-mCD8-GFP/+;; MB320C-GAL4/UAS-DIAP1
	F	UAS-mCD8-GFP/+;; MB320C-GAL4/UAS-Uba1-RNAi
	G	UAS-mCD8-GFP/+;; MB320C-GAL4/UAS-Cullin1-RNAi
Figure S6	A, B	PPK-GAL4, UAS-CD4-tdTomato/+, UAS-AKT-CA, or UAS-GSK3β-DN
Figure S7	A, B	UAS-mCD8-GFP/+; TH-D'-GAL4/Red-Repo; +/+, UAS-AKT-CA, or UAS-GSK3β-DN

894 **Main Figures**

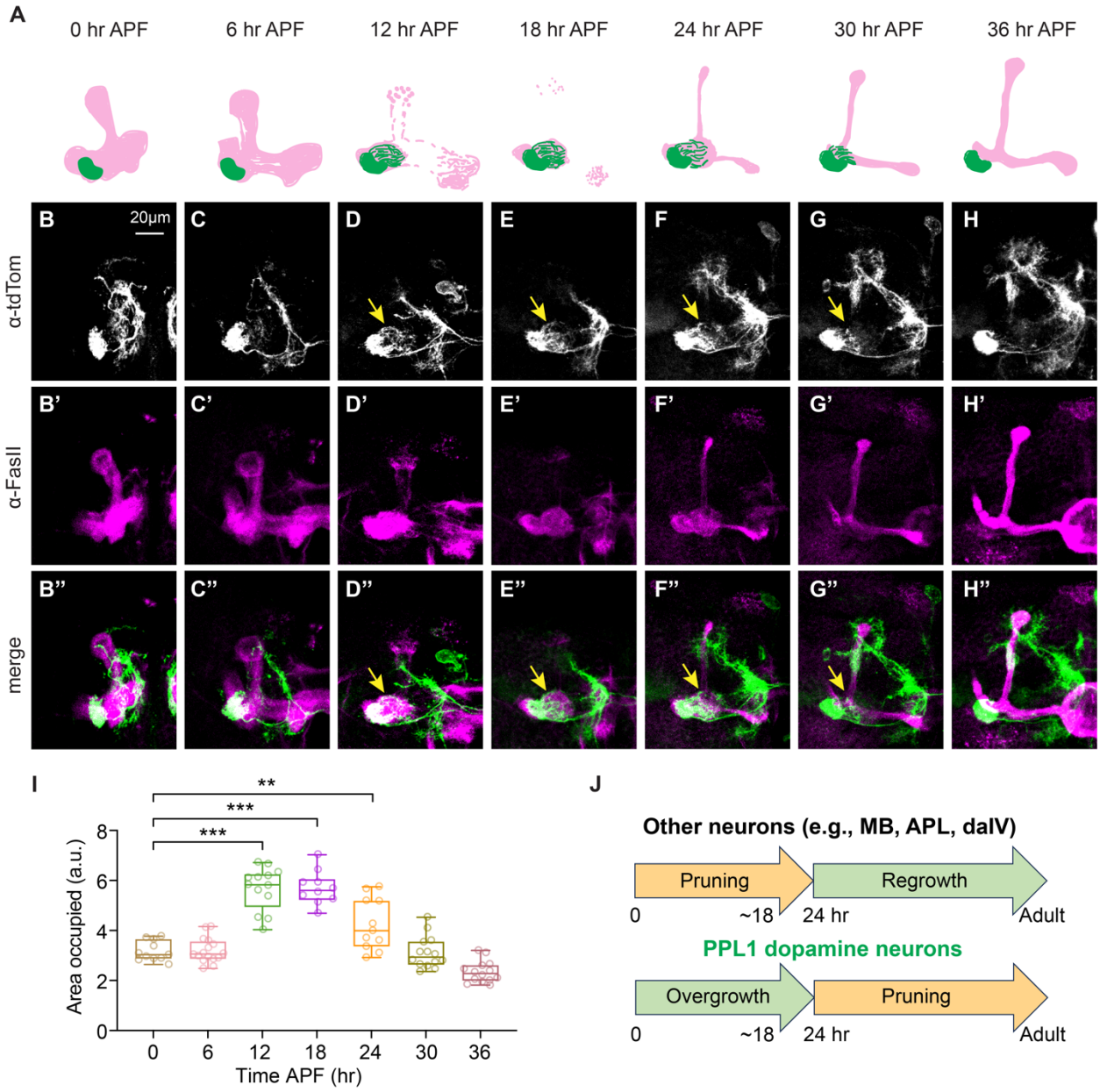

895

896 **Figure 1. Atypical developmental remodeling of dopamine neurons**

897 (A) Schematic of PPL1 DAN axon remodeling during metamorphosis. Green: MP1/MP1o
898 branch; Magenta: Mushroom body (MB) lobes labeled with anti-FasII.

899 (B-H) Confocal Z projections of brains at 0 hr (B), 6 hr (C), 12 hr (D), 18 hr (E), 24 hr (F),
900 30 hr (G), and 36 hr (H) APF expressing CD4-tdTomato driven by TH-D'-Gal4; MB lobes

are labeled with anti-FasII (B'-H'). Yellow arrows indicate the transient MP1o branch overextending from the MP1 branch into the MB MV1 region. See also Figure S1A-S1B.

(I) Quantification of the relative area occupied by MP1/MP1o branch across timepoints. $^{**}p < 0.01$, $^{***}p < 0.001$; $n = 10\text{-}16$. One-way ANOVA with Dunnett's multiple comparisons test.

(J) Summary schematic of atypical overgrowth-then-pruning developmental remodeling of DANs.

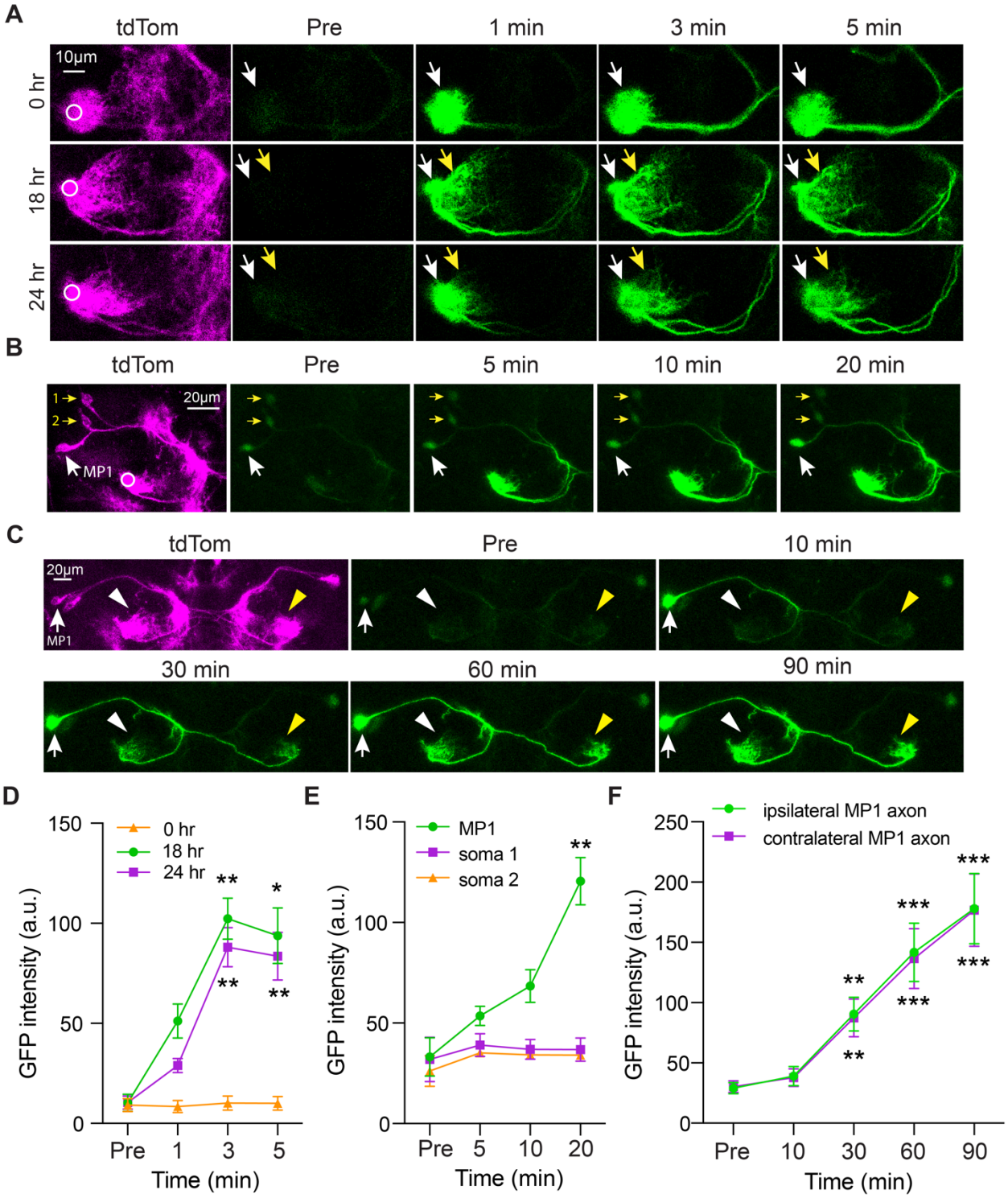

Figure 2. A single pair of DANs undergoes atypical developmental remodeling

911 (A) Photoactivation of C3PA-GFP in the MP1 branch and monitor GFP diffusion to the
912 MP1o region at 0, 18, and 24 hr APF. White circle: ROI for photoactivation; white arrow:
913 MP1 branch region; yellow arrow: MP1o region.

914 (B) Photoactivation in the MP1 branch and monitor GFP diffusion to somas at 18 hr APF.
915 White circle: ROI for photoactivation. White arrow: MP1 soma; yellow arrows: non-MP1
916 somas.

917 (C) Photoactivation in MP1 soma and monitor GFP diffusion to axons at 18 hr APF. White
918 arrow: MP1 soma; arrowheads: ipsilateral (white) and contralateral (yellow) MP1 axons.

919 (D) Quantitation of GFP fluorescence intensity in the MP1o region in (A) before (Pre) and
920 after (1-5 min) photoactivation. *$p < 0.05$, **$p < 0.01$ vs. Pre; n = 3-4; mean ± SEM;
921 Repeated measures one-way ANOVA with Dunnett's test.

922 (E) Quantitation of GFP fluorescence intensity in MP1 and two non-MP1 somas in (B)
923 before (Pre) and after (5-20 min) photoactivation. **$p < 0.01$ vs. Pre; n = 3; mean ± SEM;
924 Repeated measures one-way ANOVA with Dunnett's test.

925 (F) Quantitation of GFP fluorescence intensity in MP1 axons in (C) before (Pre) and after
926 (10-90 min) photoactivation. **$p < 0.01$, ***$p < 0.001$ vs. Pre; n = 5; mean ± SEM;
927 Repeated measures one-way ANOVA with Dunnett's test.

928

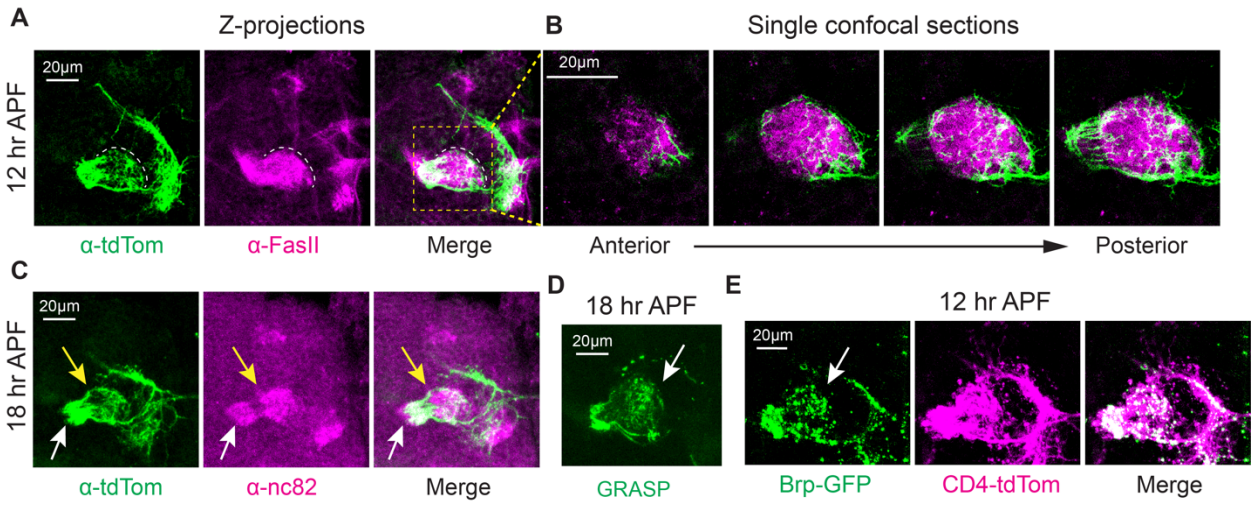

Figure 3. MP1o targets and is presynaptic to the MB

(A) Confocal Z projections of brains at 12 hr APF showing MP1o branch (TH-D'>CD4-tdTomato) innervating the MB. MB lobes are labeled with anti-FasII. Dashed lines mark the distal part of MP1o branch and the boundary of degenerating MB junction/MV1 region.

(B) High magnification single confocal sections showing the innervation pattern of MP1o branch in MB MV1 region as in the dashed box in (A).

(C) Confocal Z projections of brains at 18 hr APF expressing CD4-tdTomato driven by TH-D'-Gal4. Brain and MB lobes are visualized with anti-nc82. White arrow: MP1 region; yellow arrow: MP1o and MB MV1 regions.

(D) Confocal Z projections showing GRASP signal between MP1/MP1o and MB at 18 hr APF. White arrow: MP1o region.

(E) Confocal Z projections of brains at 12 hr APF expressing Brp-GFP and CD4-tdTomato driven by TH-D'-Gal4. White arrow: MP1o region.

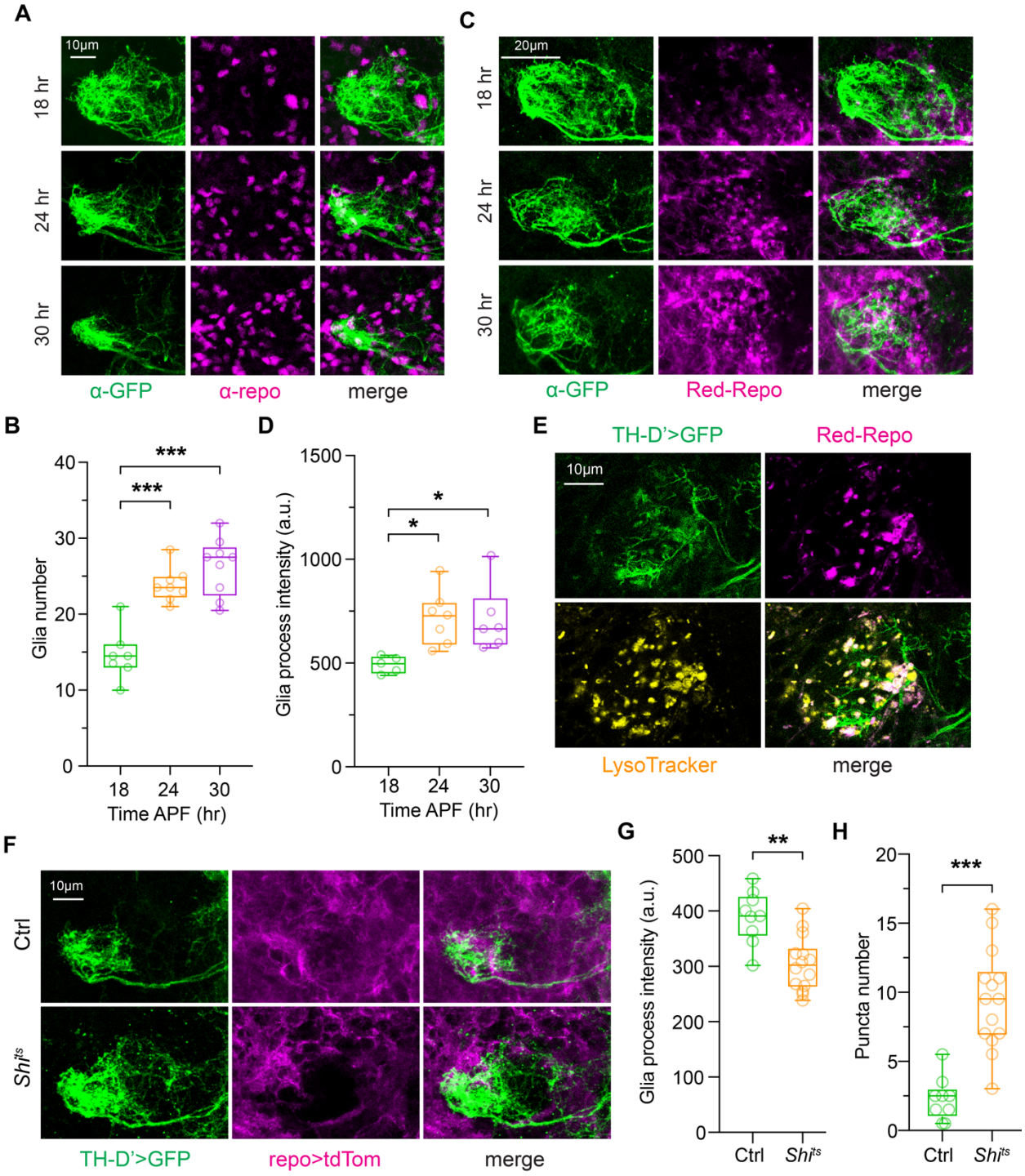

945

946 **Figure 4. Pruning of DAN axons involves glia-mediated local degeneration**

947 (A) Confocal Z projections of brains at 18 hr (top), 24 hr (middle), and 30 hr (bottom) APF
948 expressing CD4-tdGFP driven by TH-D'-Gal4. Glial nuclei are labeled with anti-Repo.

949 (B) Quantitation of glial cell numbers in the MP1/MP1o region in (A). ***$p < 0.001$; n = 7-
950 9; One-way ANOVA with Dunnett's multiple comparisons test.

951 (C) Confocal Z projections of brains at 18 hr (top), 24 hr (middle), and 30 hr (bottom) APF
952 expressing mCD8-GFP driven by TH-D'-Gal4. Glial cells/processes are labeled with Red-
953 Repo.

954 (D) Quantitation of glial process in the MP1o region in (C). *$p < 0.05$; n = 5-7; One-way
955 ANOVA with Dunnett's multiple comparisons test.

956 (E) Single confocal section showing MP1/MP1o branch (TH-D'>GFP), glial processes
957 (Red-Repo), LysoTracker, and together (merge) at 24 hr APF. See also Figure S4.

958 (F) Confocal Z projections of brains at 24 hr APF in control (top) and *shi*^{ts} (bottom) groups.
959 MP1 DANs labeled with TH-D'-GAL4>UAS-myr-GFP; glia labeled with Repo-
960 QF2>QUAS-mtdTomato-3XHA, with or without QUAS-*shi*^{ts}; Control group lacking QUAS-
961 *shi*^{ts} was subjected to the same temperature shift protocol as *shi*^{ts} group.

962 (G-H) Quantitation of glial process (G) and GFP-positive puncta (H) in MP1o region in (F).
963 **$p < 0.01$, ***$p < 0.001$; n = 9-14; Mann Whitney test.

964

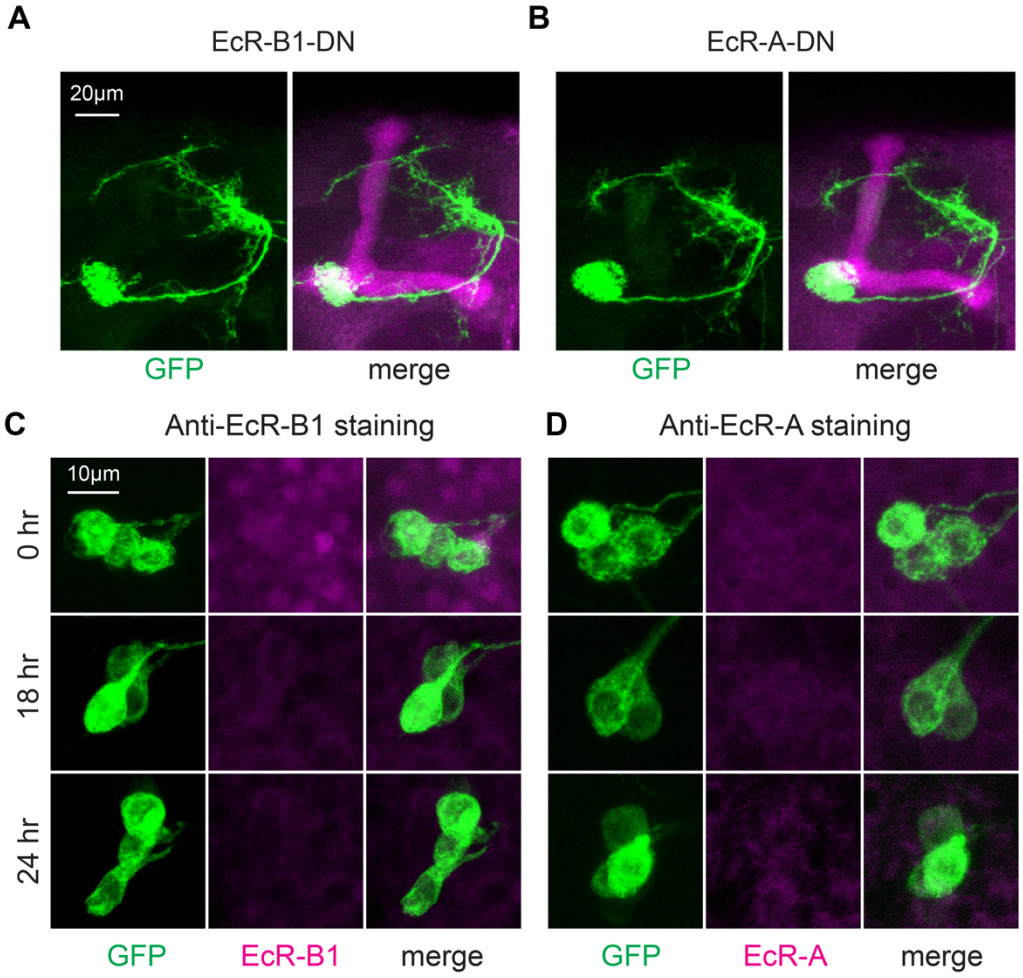

965

966 **Figure 5. Canonical ecdysone signaling is dispensable for DAN axon pruning**

967 (A-B) Confocal Z projections of adult brains expressing mCD8-GFP and EcR-B1-DN (A)
968 or EcR-A-DN (B) driven by MB320C-Gal4. Magenta: MB lobes labeled with anti-FasII. No
969 MP1o branches observed.

970 (C-D) Confocal Z projections of brains at 0 hr (top), 18 hr (middle), and 24 hr (bottom)
971 APF showing somas of MP1 DANs (TH-D'>mCD8-GFP) and immunostaining for EcR-B1
972 or EcR-A (D). EcR expression is not detected above background in MP1 DANs at any
973 time point. See also Figure S5.

974

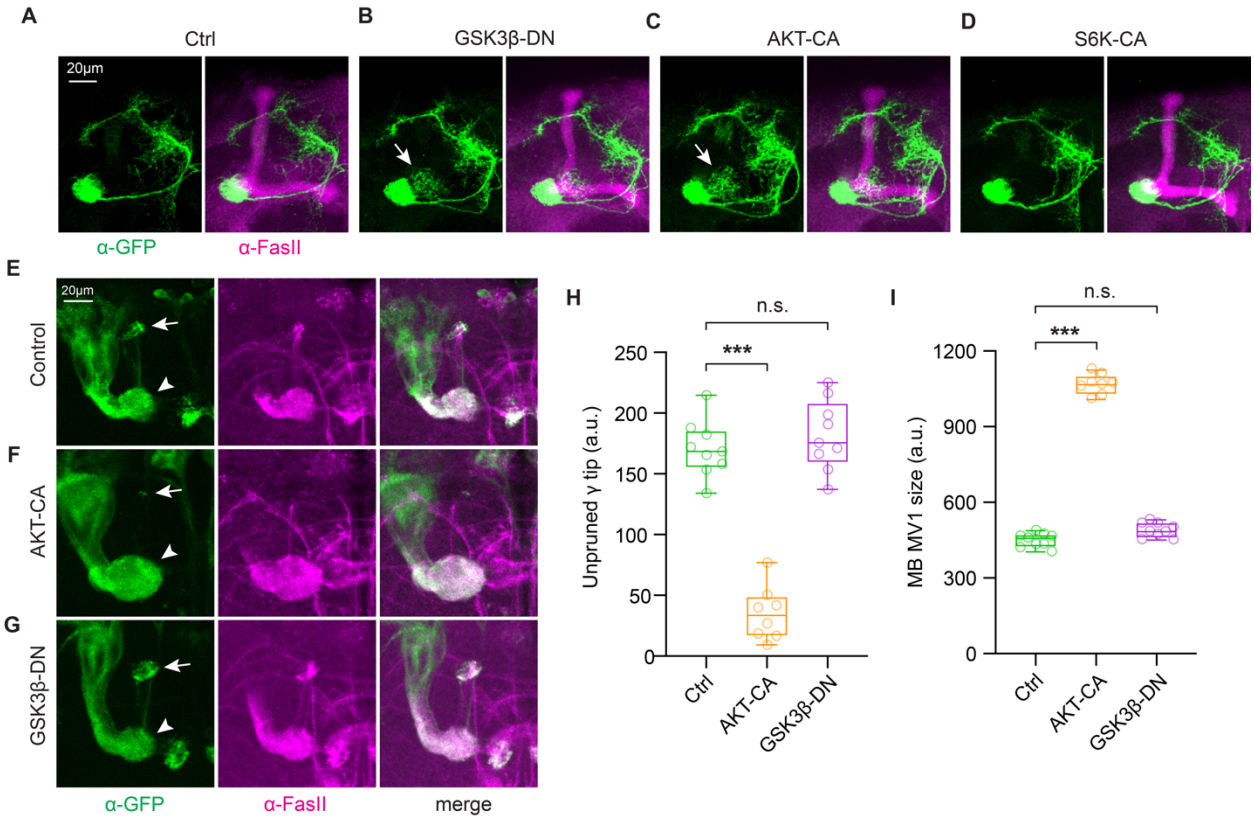

975

976 **Figure 6. Roles of AKT-GSK3β signaling in developmental remodeling**

977 (A-D) Confocal Z projections of adult brains expressing mCD8-GFP driven by MB320C-
978 Gal4. Expression of GSK3β-DN (B) and AKT-CA (C), but not S6K-CA (D) in MP1 DANs
979 impairs pruning of MP1o branch compared to control (A). MB lobes labeled with anti-FasII.
980 White arrow indicates persistent MP1o branch in GSK3β-DN and AKT-CA groups.

981 (E-G) Differential effects of AKT-CA (F) and GSK3β-DN (G) on MB γ neuron pruning. MB
982 labeled with 201Y-Gal4>mCD8-GFP. White arrow: distal tip of MB γ neuron vertical lobe;
983 white arrowhead: unpruned MB junction/MV1 region.

984 (H-I) Quantitation of the unpruned distal tip of MB vertical lobe (H) and junction/MV1 area
985 (I) in control (E), AKT-CA (F), and GSK3β-DN (G) groups at 18 hr APF. ***$p < 0.001$; n.s.,
986 not significant; n = 8-9; One-way ANOVA with Dunnett's multiple comparisons test.

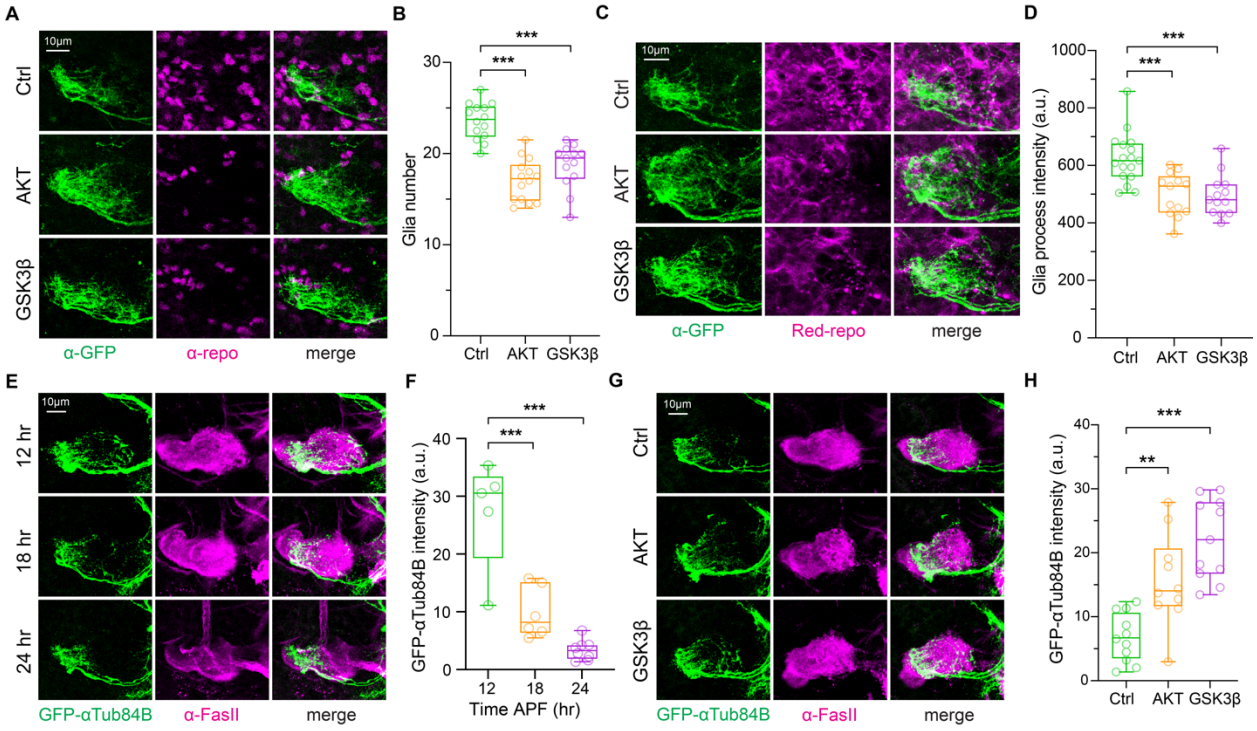

Figure 7. AKT-GSK3β signaling modulates microtubule cytoskeleton and glial activities during DAN axon degeneration

(A) Confocal Z projections of brains at 24 hr APF expressing mCD8-GFP driven by TH-D'-Gal4 in control (top), AKT-CA (middle), and GSK3β-DN (bottom) groups. Glial nuclei labeled with anti-Repo.

(B) Quantitation of glial cell number in MP1/MP1o region in (A). ***$p < 0.001$; n = 13-14; One-way ANOVA with Dunnett's multiple comparisons test.

(C) Confocal Z projections as in (A) but with glial cells/processes labeled with Red-Repo.

(D) Quantitation of glial process in MP1o region in (C). ***$p < 0.001$; n = 13-17; One-way ANOVA with Dunnett's multiple comparisons test.

(E) Confocal Z projections of brains at 12 hr (top), 18 hr (middle), and 24 hr (bottom) APF expressing GFP-αTub84B driven by TH-D'-Gal4. MB lobes labeled with anti-FasII.

(F) Quantitation of GFP-αTub84B signal intensity in MP1o region in (E). ***$p < 0.001$; n = 5-8; One-way ANOVA with Tukey's multiple comparisons test.

1002 (G) Confocal Z projections of brains at 18 hr APF expressing GFP-αTub84B driven by
1003 TH-D'-Gal4 in control (top), AKT-CA (middle), and GSK3β-DN (bottom) groups. MB lobes
1004 labeled with anti-FasII.

1005 (H) Quantitation of GFP-αTub84B signal intensity in MP1o region in (G). $^{**}p < 0.01$, $^{***}p$
1006 < 0.001; $n = 10\text{-}12$; One-way ANOVA with Tukey's multiple comparisons test.

1007

1008 **Supplementary Figures**

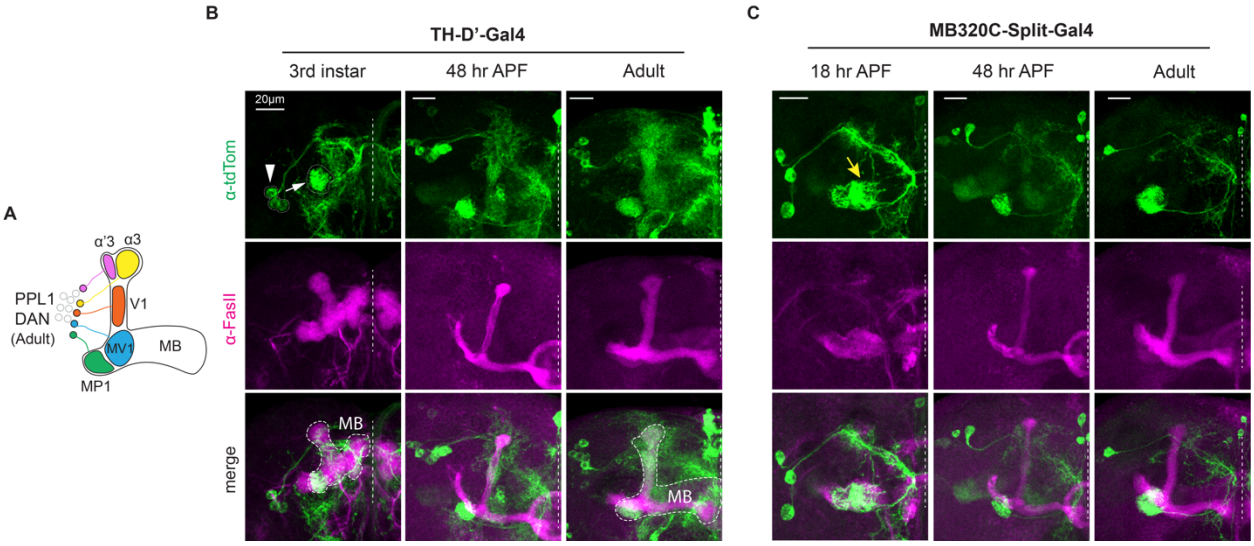

1009

1010 **Figure S1. Atypical developmental remodeling of DANs, related to Figure 1**

1011 (A) Schematic of PPL1 DAN innervation patterns in the adult brain.

1012 (B) Confocal Z projections of brains from 3rd instar larvae (left), 48 hr APF (middle), and
1013 adults (right) expressing CD4-tdTomato driven by TH-D'-Gal4. MB lobes are labeled with
1014 anti-FasII. White arrow: MP1 branch; white arrowhead: somas; dashed circles: MB.

1015 (C) Confocal Z projections of brains at 18 hr (left), 48 hr (middle), and adult (right)
1016 expressing CD4-tdTomato driven by MB320C-Split-Gal4. Yellow arrow: MP1o branch at
1017 18 hr APF.

1018

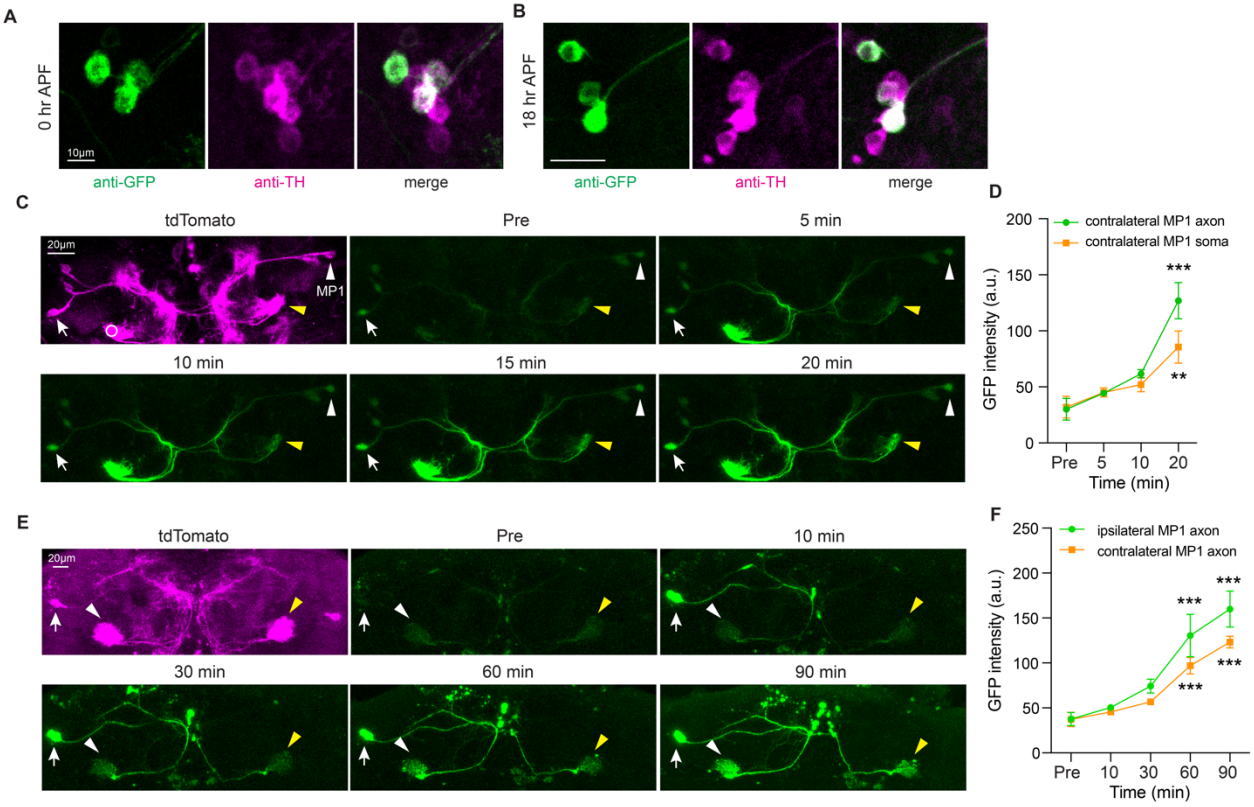

Figure S2. A single pair of DANs undergoes atypical developmental remodeling, related to Figure 2

(A-B) Anti-TH immunostaining confirms that all three TH-D'-Gal4-labeled somas are TH-positive at 0 hr (A) and 18 hr (B) APF.

(C) Photoactivation of C3PA-GFP in MP1 branch and monitor GFP diffusion to contralateral MP1 axon and soma (same brain as Figure 2C). White circle: ROI for photoactivation. White arrow: ipsilateral MP1 soma; white arrowhead: contralateral MP1 soma; yellow arrowhead: contralateral MP1 axon.

(D) Quantitation of GFP fluorescence intensity in contralateral MP1 axon and soma in (C) before (Pre) and after (5-20 min) photoactivation. $^{**}p < 0.01$, $^{***}p < 0.001$ vs. Pre; $n = 3$; mean ± SEM; Repeated measures one-way ANOVA with Dunnett's test.

1031 (E) Photoactivation in MP1 soma and monitor GFP diffusion to ipsilateral and contralateral
1032 MP1 axons in adult. White arrow: ipsilateral MP1 soma; white arrowhead: ipsilateral MP1
1033 axon; yellow arrowhead: contralateral MP1 axon.

1034 (F) Quantitation of GFP fluorescence intensity in ipsilateral and contralateral MP1 axons
1035 in (E) before (Pre) and after (10-90 min) photoactivation. ***$p < 0.001$ vs. Pre; $n = 4$; mean
1036 ± SEM; Repeated measures one-way ANOVA with Dunnett's test.

1037

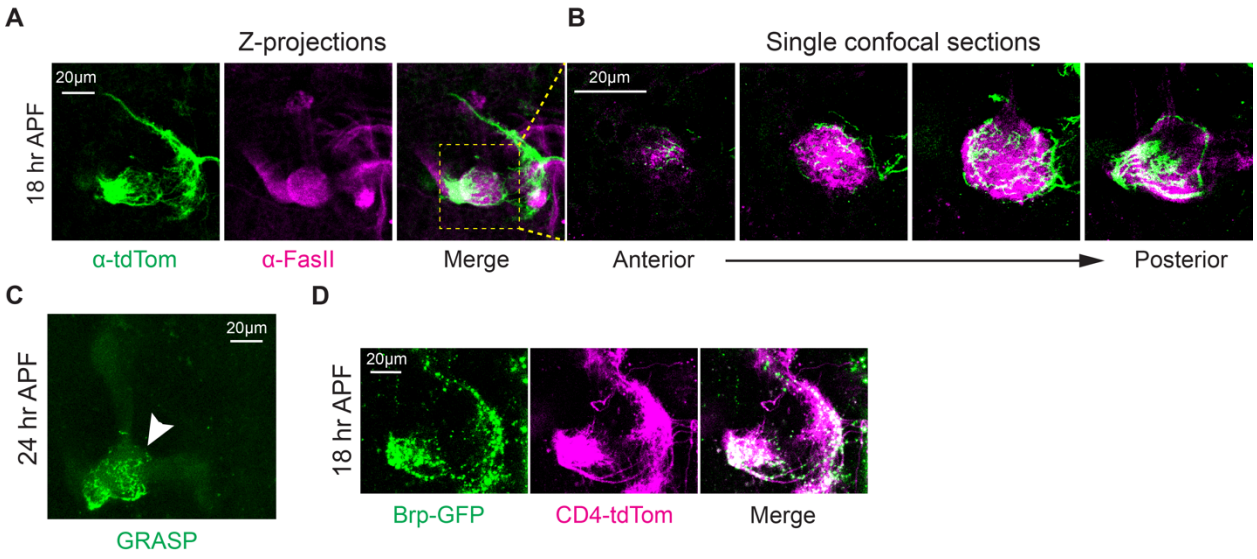

Figure S3. MP1o targets and is presynaptic to the MB, related to Figure 3

(A) Confocal Z projections of brains at 18 hr APF expressing CD4-tdTomato driven by TH-D'-Gal4 with MB lobes labeled by anti-FasII.

(B) High magnification single confocal sections showing the innervation pattern of MP1o branch in MB MV1 region as in the dashed box in (A).

(C) Confocal Z projections showing GRASP signal between MP1/MP1o and MB at 24 hr APF. White arrowhead: MP1o region.

(D) Confocal Z projections of brains at 18 hr APF expressing Brp-GFP and CD4-tdTomato driven by TH-D'-Gal4.

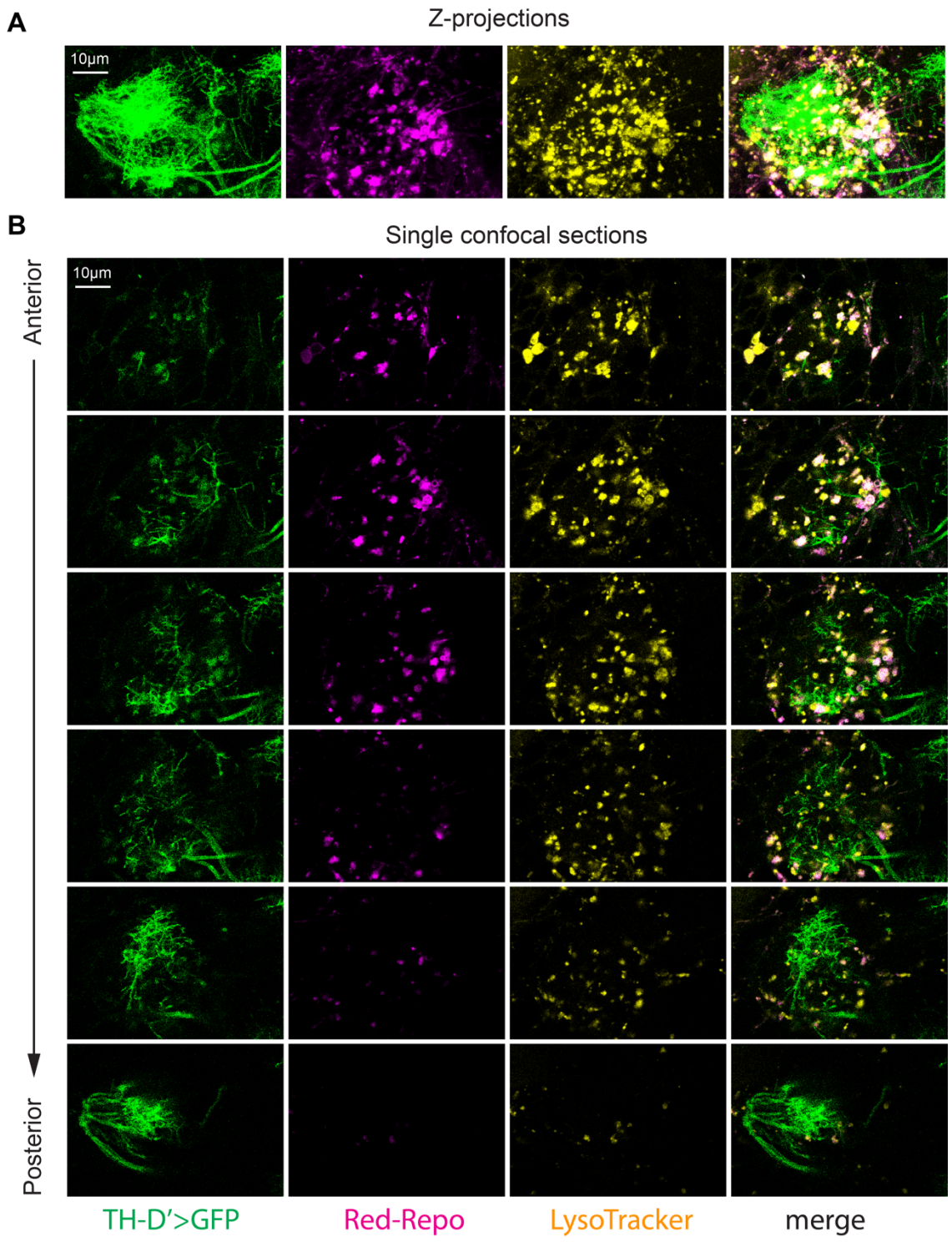

1049

1050 **Figure S4. Pruning of DAN axons involves glia-mediated local degeneration, related**

1051 **to Figure 4**

1052 (A-B) Confocal Z projections (A) and single confocal sections (B) showing MP1/MP1o
1053 branch (TH-D'>GFP), glial processes (Red-Repo), LysoTracker, and together (merge) at
1054 24 hr APF.

1055

1056

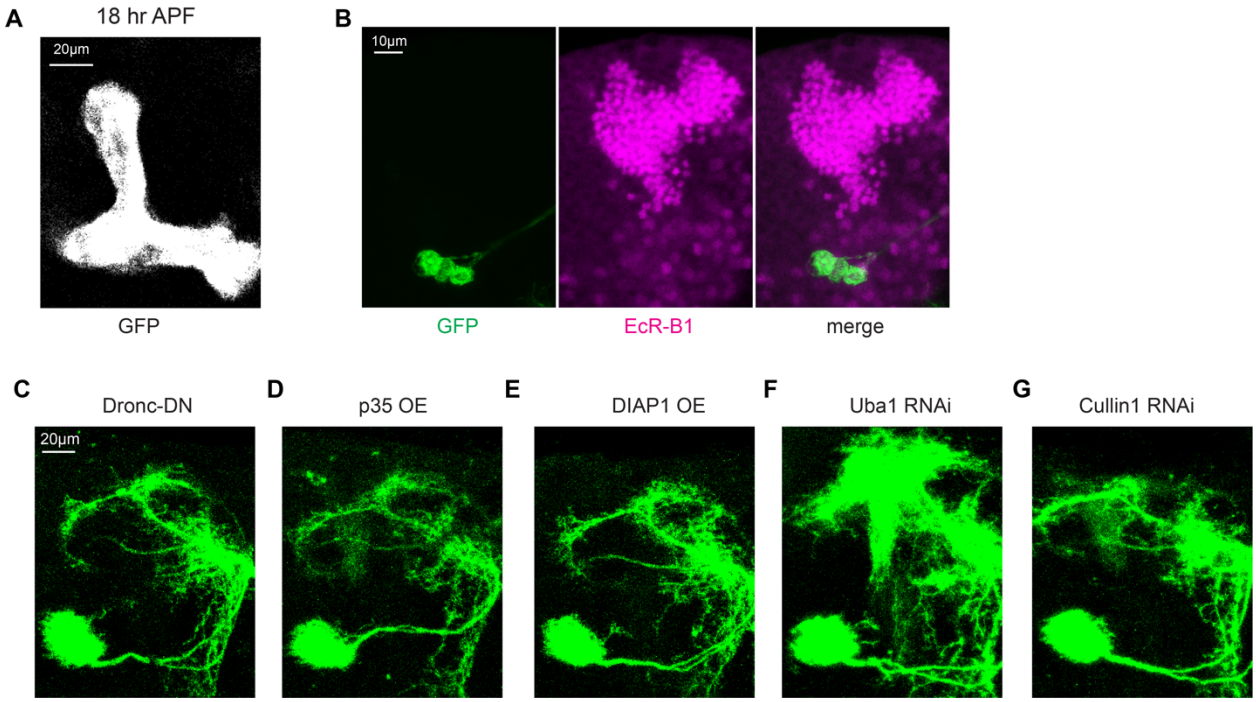

Figure S5. Canonical ecdysone signaling, caspase activity, and UPS are dispensable for DAN axon pruning, related to Figure 5

(A) Confocal Z projections of MB lobes at 18 hr APF expressing mCD8-GFP and EcR-B1-DN driven by 201Y-Gal4.

(B) EcR-B1 protein expression in TH-D'>mCD8-GFP brains at 0 hr APF.

(C-G) Expression of Dronc-DN (C), overexpression of p35 (D) and DIAP1 (E), and RNAi knockdown of Uba1 (F) and Cullin1 (G) do not impair MP1o pruning. Adult stage MP1 DANs are visualized with MB320C-Gal4 driving mCD8-GFP.

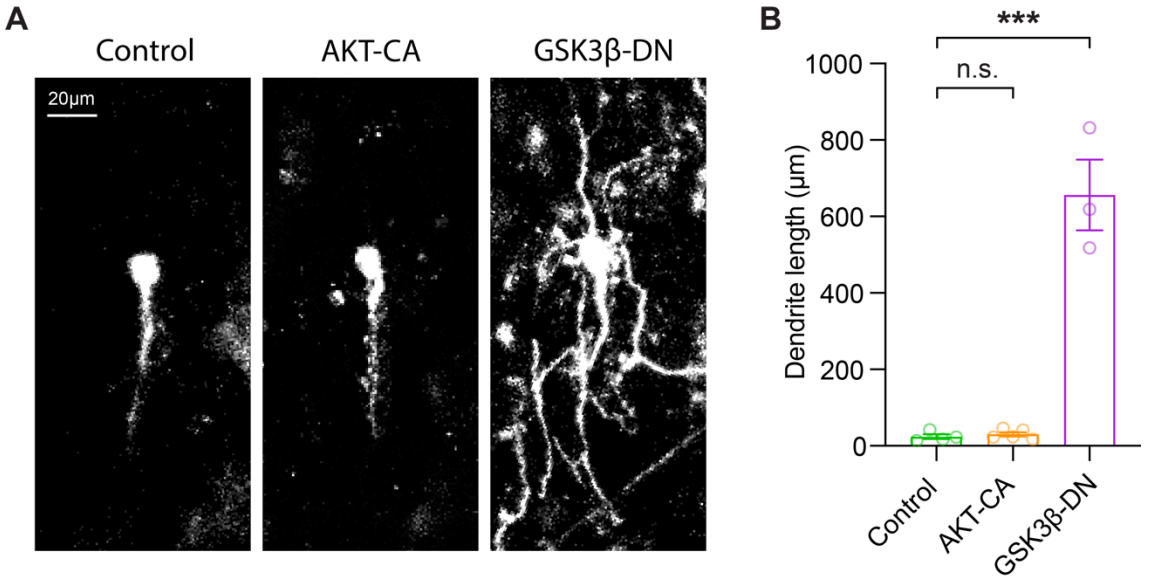

1067

1068 **Figure S6. Differential roles of AKT and GSK3β in dendrite pruning of daIV neurons,**
1069 **related to Figure 6**

1070 (A) Confocal Z projections of daIV neurons expressing CD4-tdTomato driven by PPK-
1071 Gal4 at 18 hr APF in control (left), AKT-CA (middle), and GSK3β-DN (right) groups.

1072 (B) Quantitation of total dendrite length in (A). ***$p < 0.001$; n.s., not significant; n = 3-5;
1073 mean ± SEM; One-way ANOVA with Dunnett's multiple comparisons test.

1074

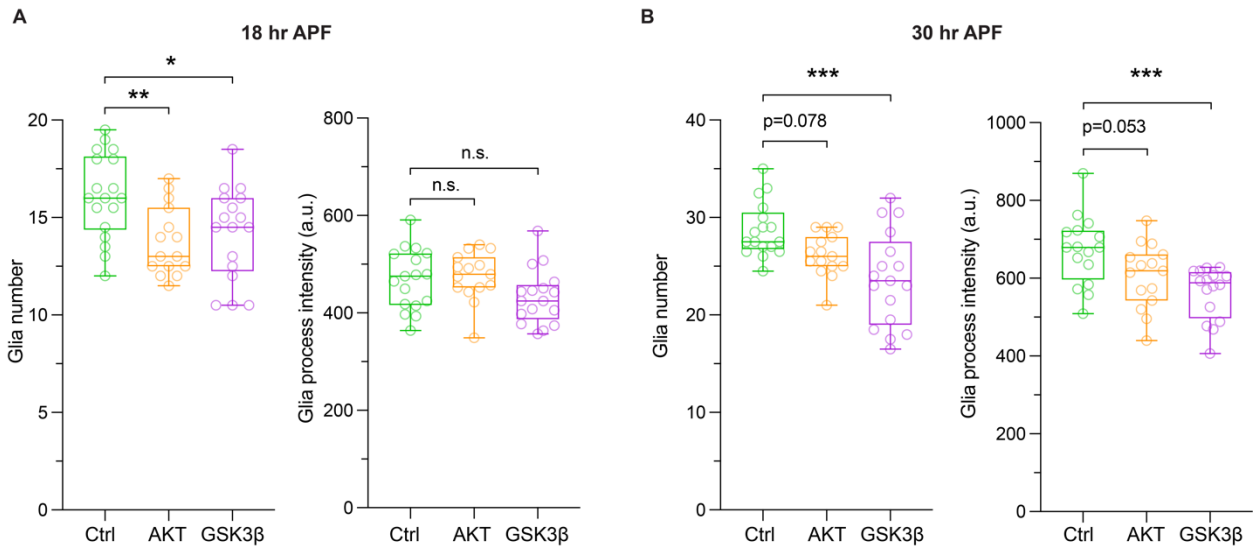

Figure S7. Quantification of glial dynamics during DAN axon degeneration, related to Figure 7

(A) Quantitation of glial cell number (left) and process intensity (right) in the MP1/MP1o region in control, AKT-CA, and GSK3β-DN groups at 18 hr APF. *$p < 0.05$, **$p < 0.01$; n = 15-18; One-way ANOVA with Dunnett's multiple comparisons test.

(B) Quantitation of glial cell number (left) and process intensity (right) in the MP1/MP1o region in control, AKT-CA, and GSK3β-DN groups at 30 hr APF. ***$p < 0.001$; n = 15-17; One-way ANOVA with Dunnett's multiple comparisons test.

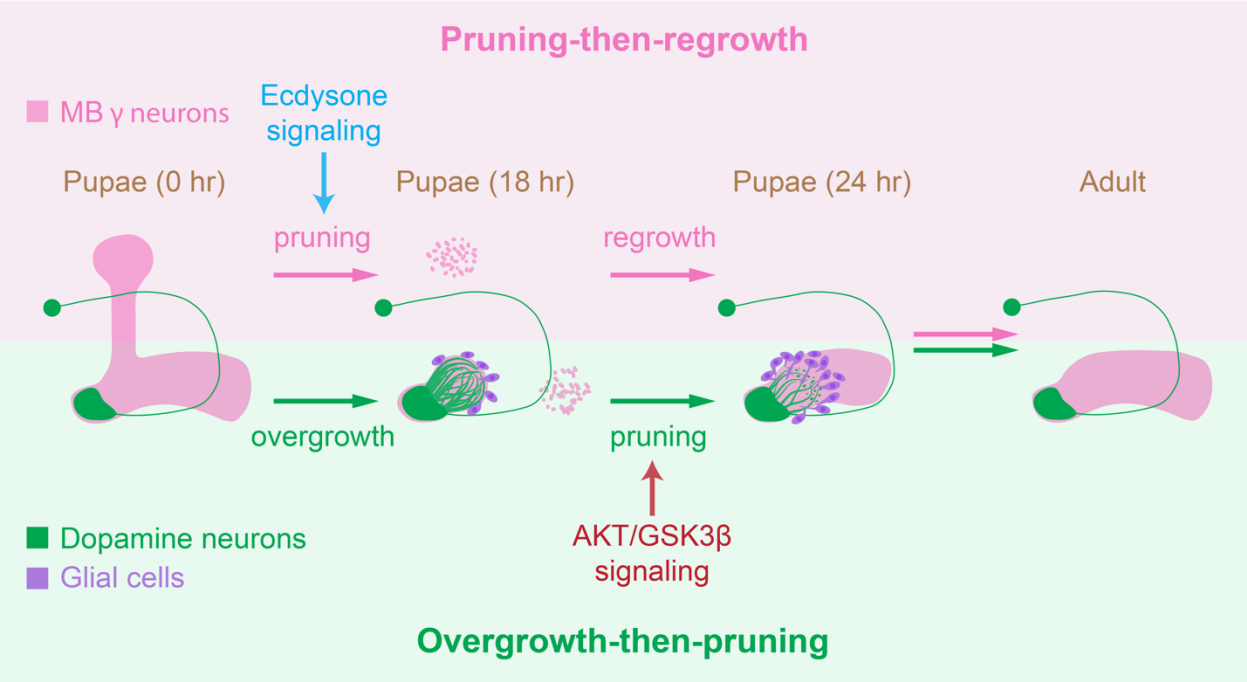

Figure S8. Model

In contrast to the stereotypical pruning-then-regrowth remodeling paradigm observed in most neuron types – such as MB γ neurons (illustrated here), APL neurons, PNs, and daIV neurons – MP1 DANs, which innervate the MB heel region, undergo an atypical overgrowth-then-pruning trajectory during *Drosophila* metamorphosis. Moreover, pruning of MP1 DAN axons occurs independently of the canonical ecdysone-EcR signaling pathway and instead involves neuron-intrinsic AKT-GSK3β signaling and extrinsic glial activity.

1095 **Video S1. 3D reconstruction of MP1/MP1o branch and MB axons at 12 hr APF,**
1096 **related to Figure 3A.**

1097 3D rendering of MP1/MP1o branch and MB lobes at 12 hr APF. Green: MP1/MP1o axon
1098 branches (TH-D'>CD4-tdTomato); magenta: MB peduncle (MP1) and junction/MV1
1099 region (anti-FasII). MP1o projects into MB MV1 region.